Dissertations and Theses

11-2017

Development and Characterization of Piezoresistive Nanocomposites for Sensing Applications

Muhammad Anees

Follow this and additional works at: https://commons.erau.edu/edt

Part of the Aerospace Engineering Commons

DEVELOPMENT AND CHARACTERIZATION OF PIEZORESISTIVE

NANOCOMPOSITES FOR SENSING APPLICATIONS

A Thesis

Submitted to the Faculty

of

Embry-Riddle Aeronautical University

by

Muhammad Anees

In Partial Fulfillment of the

Requirements for the Degree

of

Master of Science in Aerospace Engineering

November 2017

Embry-Riddle Aeronautical University

Daytona Beach, Florida

DEVELOPMENT AND CHARACTERIZATION OF PIEZORESISTIVE NANOCOMPOSITES FOR SENSING APPLICATIONS

by

Muhammad Anees

A Thesis prepared under the direction of the candidate's committee chairman, Dr. Daewon Kim and Dr. Sirish Namilae, Department of Aerospace Engineering, and has been approved by the members of the thesis committee. It was submitted to the School of Graduate Studies and Research and was accepted in partial fulfillment of the requirements for the degree of Master of Science in Aerospace Engineering.
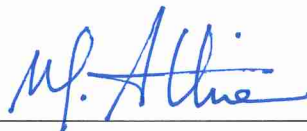
THESIS COMMITTEE

Chairman, Dr. Daewon Kim

Co-Chairman, Dr. Sirish Namilae

Member, Dr. Marwan Al-Haik

Graduate Program Coordinator, Dr. Magdy Attia
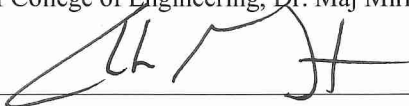
11·29· 2017
Date

Dean of College of Engineering, Dr. Maj Mirmirani

11/29/2017
Date

Vice Chancellor, Academic Support, Dr. Christopher Grant

11/30/17
Date

ACKNOWLEDGMENTS

TABLE OF CONTENTS

LIST OF TABLES

LIST OF FIGURES

SYMBOLS

R	resistance
I	current
ΔV	voltage drop
ρ	resistivity
w	width of nanocomposites
t	thickness of nanocomposites
L	length of nanocomposites
V	Applied voltage
ε	strain
A	surface area of nanocomposite

ABBREVIATIONS

CNT	Carbon nanotubes
GNP	Graphene nanoplatelets
TML	Total mass loss
2216 Trans	Scotch weld 3M 2216 B/A Translucent epoxy
2216 Gray	Scotch weld 3M 2216 B/A Gray epoxy
WS	West systems epoxy
SWNT	Single walled carbon nanotube
MWNT	Multiwalled carbon nanotube
DIC	Digital image correlation

ABSTRACT

Anees, Muhammad MSAE, Embry-Riddle Aeronautical University, November 2017. Development and characterization of piezoresistive nanocomposites for sensing applications.

Carbon nanotube based hybrid nanocomposites are known to exhibit remarkable electrical and mechanical properties with many potentials in strain and damage sensing applications. In this work, we fabricate hybrid nanocomposites with carbon nanotube (CNT) sheet and graphene nanoplatelets (GNP) as fillers with epoxy matrix. An improvement in both electrical conductivity and piezoresistivity is observed with the combination of CNTs and GNPs, indicating the formation of efficient hybrid conductive networks for strain and electrical transfer in the material. Different matrix materials have been compared to investigate the effect of matrix and to choose the one that yields increased strains, flexibility, and electromechanical response. The electromechanical behavior of the hybrid composites is investigated both under static and dynamic loading at various frequencies with induced levels of strains, and has shown positive response under all tested conditions. Digital image correlation has been used to investigate the strain variation within the specimen both during static and dynamic testing. As these sensors will be tested for damage sensing in space applications for inflatable habitat under Micrometeoroid and Orbital Debris (MMOD) impact, the sensitivity of the sensor with 3 mm impact holes is evaluated using four point probe electrical resistivity measurements. An array of these sensors when sandwiched between soft good layers in a space habitat can act as a damage detection layer for inflatable structures. A computer program is developed to determine the event of impact, its severity and the location on the sensing layer for active

health monitoring. Outgassing testing has been performed to evaluate the Total Mass Loss (TML) of the nanocomposite in space environment. Our results indicate that these hybrid nanocomposites exhibit a distinct piezo resistive response which can be beneficial for potential strain, vibration, and damage sensing applications.

1. Introduction

Composites is one of the widest growing structural materials especially in aerospace applications due to their light weight and high mechanical strength. Tailoring their properties by varying the amount and orientation of fibers by modification of matrix material to achieve desirable properties makes them versatile for a variety of applications. Due to their superior properties and significant cost saving over the life of the structure, advanced commercial and military aircrafts as well as spacecraft are using more than 50% of composite material in their structure.

All aerospace structures are prone to damage and wear during their life, and are therefore inspected timely to ensure their integrity. This is either through nondestructive testing or installation of sensors to identify of change in properties of the structure which can be used for indication of damage. Structural health monitoring (SHM) is an emerging field which involves installation of inbuilt sensors on the structure and their continuous monitoring so that they can give information about structural health and remaining life. Development of advanced sensors that can be easily integrated into existing structure with minimal modification is an important and developing areas of research.

Space structures and materials are prone to much higher challenges due to extreme environment such as high temperature variation, radiation and outgassing. Therefore, space grade materials have unique requirements to perform well under these environmental conditions. The outer structure exposed to space is also prone to damage caused by Micro Meteoroid and Orbital Debris (MMOD) and therefore should be able to withstand these impacts without affecting the inner structure.

Carbon fiber reinforced composites are one of the most widely used composites

that have much high mechanical, thermal and fatigue strength. Carbon nanotubes (CNTs) are allotropes of carbon with cylindrical structure in nanometer scale dimensions. It is a novel material that possess extremely high mechanical strength in combination with electrical and thermal conductivity and stability. CNT based composites, also called nanocomposites, can show unique electromechanical behavior depending on the material design of the composite, which is unlikely with other filler materials. These properties can be used in the development of sensors and other smart materials that can exhibit multifunctional behavior in the structures.

CNTs can be of two types, i.e. single wall carbon nanotube (SWNT) and multi-wall carbon nanotube (MWNT). SWNTs are single cylindrical layer of graphene, which is made up of a hexagonal lattice of carbon atoms in a honeycomb like structure. Several layers of graphene stacked together form graphene sheet. MWNTs consist of nested cylindrical tubes of graphene with increasing diameter. MWNTs can be interwoven by utilizing internal Van der Waals forces to develop a thin membrane of free standing CNTs called buckypaper. Figure 1.1 shows all these different forms of carbon nanostructure.

(a)	(b)	(c)	(d)	(e)
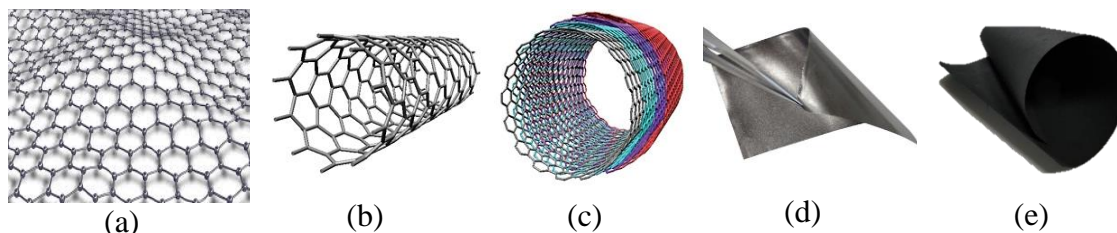
Figure 1.1 Different forms of carbon nanostructure (a) Graphene structure (b) SWNT (c) MWNT (d) Graphaite sheet (e) Buckypaper (Aqel et al. 2012)

This study is an attempt to develop CNT based nanocomposites, which consist of one or more than one form of CNT fillers, i.e. MWNTs and Graphene Nano platelets (GNP) fillers, with epoxy matrices. Due to the conductive CNT structure embedded in the matrix,

the electrical resistance of the nanocomposite varies with applied mechanical loading and this phenomena is called piezoresistivity. This phenomenon is exploited for sensing of structural behavior during mechanical loadings, such as strains and vibrations, and to develop these nanocomposites as sensors. Change in the resistance of these nanocomposites also occurs due to the change in conductive area caused by addition of holes. This phenomenon is used to develop these nanocomposites for sensing of damage caused by MMOD in space environment. Effect of matrix behavior on piezoresistivity and flexibility of the nanocomposite sensors have been investigated. These nanocomposites have been characterized as flexible strain sensors, vibration sensors, and damage sensors caused due to MMOD impacts. Additional applications also include embedded flexible damage sensors for cracks in composites and composite repair.

1.1. Motivation

CNT/epoxy and CNT+GNP/epoxy based hybrid composites have been proven to exhibit strain sensing capabilities (Jiukun Li and Namilae 2016). Their primary advantage is that they can be bonded on or integrated between the layers of the composite structures inducing minimal changes in the structure system. However, these nanocomposites cannot undergo large deformations and are brittle in nature. These characteristics limit their application for expandable/foldable structures such as inflatable structures for space habitat. Therefore, there is a room for improvement to extend these sensor performance for high strain and high flexible environments. Moreover, it is not known how these nanocomposites perform when the applied loading is cyclic in nature, i.e. vibrations and cyclic loadings. If the response of these nanocomposites is characterized for cyclic loading and is found out to be satisfactory, their sensing capabilities can be extended. These

nanocomposites are also explored for their potential usage in damage sensing in the inflatable structures against MMOD impacts as a part of work done for NASA's SBIR grant for Phase I and II. Integration of sensors to develop integrated structural health monitoring would require a method for integration, sensing, and indication of damage. Space materials are prone to outgassing, therefore outgassing testing of these nanocomposites should also be conducted to study for suitability of these sensors in the space environment

1.2. Problem Statement

The objective of this study is develop CNT based piezoresistive hybrid nanocomposites and characterize their behavior for increased strain sensing, vibration sensing, and damage detection while keeping them flexible enough to be folded and packed. These efforts are to investigate their suitability as the sensing layers in space environments, especially as the skin layers of inflatable structures.

1.3. Research Objectives

In order to address these challenges, CNT/GNP/epoxy based nanocomposites shall be developed and following specific tasks shall be performed.

1. Investigate the effect of different matrix materials on mechanical and piezoresistive response of the nanocomposite under tensile loading, and qualify them as strain sensors with increased strain capabilities through tensile testing.

2. Investigate the effect of cyclic loading on the specimen and its suitability to sense vibrational deformations through vibration testing.

3. Investigate the strain variation with the specimen under applied static or dynamic

loading to understand the material behavior through technique of digital image correlation.

4. Investigate the effect of frequency and temperature on the material behavior to find out the suitable working range for vibration sensing through dynamic mechanical analysis.

5. Investigate the response of the nanocomposites as damage sensors with holes caused by MMOD impact, through puncture hole testing.

6. Develop a scheme for incorporation of nanocomposite inside walls of inflatable structure for real time health monitoring against MMOD impacts.

7. Investigate the outgassing properties of the nanocomposite sensors for its potential usage in space environment.

2. Nanocomposite Development and Tensile Testing

CNTs were first discovered in 1991 as MWNTs (Iijima, 1991) and their variants SWNT were discovered in 1993 (Iijima et. al. 1993) (Bethune et al., 1993) and since then they have been one of the most researched materials due to their extraordinary electrical, mechanical, and thermal properties. Their electrical conductivity is almost 1000 times to that of copper wire (Salvetat et al., 1999). The elastic modulus of CNTs is about 1.2TPa and their strength can go up to 200 GPa, which is almost 100 times strength of steel. Moreover, their density is quite low, i.e. about 1.4 g/cm^3 which is almost 5-6 times less than steel (Bethune et al., 1993). They have double the thermal conductivity of diamond, and stable up to 750°C in air and up to 2000°C in vacuum (Berber, Kwon, & Tománek, 2000). Owing to these superior properties, they are widely used as fillers in the composites. In composites it is essential to effectively transfer the load from the matrix to the fillers whether it is electrical, mechanical or thermal load. Moreover, the effectiveness of CNTs in composites also depends on their orientation, adhesion and surface therefore it is important to consider these factors while studying CNT based composites.

2.1. Literature review

Besides their superior properties, CNTs also show piezoresistivity, i.e. change in their electrical conductivity upon mechanical deformation (Tombler et al., 2000). This unlocks their potential to be used in variety of strain sensing and actuation applications. The response can be linear and nonlinear depending on the matrix material. Several references can be found in the literature in this regard. CNTs are sandwiched between two layers of Parylene-C, with a polyimide layer as the sensing surface to develop flexible strain sensor (Huang et al. 2012). CNT/polyelectrolyte composite have been prepared to

develop multifunctional material for measuring strain and corrosion (Loh et al. 2007). CNT nanocomposites with biodegradable polymers (Mittal 2011) and SWNT/polymethylmethacrylate composite have been developed for strain sensing (Kang et al. 2006), MWNTs/glass fiber epoxy composite, (Yuezhen Bin et al. 2003) (Thostenson and Chou 2006) CNT/polyvinylidifluorid (PVDF) (J. M. Park et al., 2013), CNT/poly(ionic liquid)s, (Gendron et al. 2015) composites have been prepared and shown to possess strain sensing capabilities.

Both SWNT and MWNT buckypaper have also been used with liquid crystalline polymer (Parmax) matrices (Chang et al. 2013a), buckypaper/cyclic butylene terephthalate (pCBT), (Z. Li, et al. 2015) buckypaper/organic polymers, such as poly(vinyl alcohol), poly(vinyl pyrrolidone), and poly(styrene (Coleman et al. 2003) composites to develop strain sensing nanocomposite sensors. The elastic modulus of the buckypaper/epoxy based nanocomposites is reported to vary from 1.1 GPa to 33 GPa while the tensile strength vary from 13 MPa to 387 MPa. (Coleman et al. 2003) (Sreekumar et al. 2003) (Pham et al. 2008) (Chang et al. 2013a) This high variation in mechanical properties makes it evident that they are highly dependent on the matrix material as well as the types and amount of CNTs used.

Similarly, the electrical performance of the nanocomposite is also highly dependent on various factors such as weight percentage (wt%) of CNTs in the matrix, filler size, matrix material, impurities, and percolation threshold. Percolation threshold is the minimum amount of CNTs required in the composite to form a continuous electrical network and it also varies due to above mentioned reason. The resistivity of the nanocomposites is found to be in the range of 1.9×10^{-5} to 39.2×10^{-5} Ωm (Wang 2005) (Chapartegui et al. 2012) (Chapartegui et al. 2013).

CNTs have been reported to have excellent piezo-resistive response, which can be expressed by gauge factor. Gauge factor can be expressed as

$$Gauge\ Factor = \frac{\Delta R}{R} \times \frac{1}{\varepsilon}$$

where ΔR is the change in resistance, R is the initial resistance, and ε is the strain. Gauge factor of pure SWNTs vary from 400 to 2900 (C. Stampfer et al. 2006), which is extremely high as compared to gauge factor of typical strain gauge, i.e. 2. Such high gauge factor allows them to be an excellent material to develop them as strain sensor which can be done by incorporating them in a suitable matrix material. However, in composites, the gauge factor significantly drops to the range of 0.5 to 22.4 (Zhao et al. 2010) (Hu et al. 2010). The change in resistance with applied loading of CNT nanocomposites is a result of interactions between CNTs and the matrix instead of intrinsic property of individual CNTs (Hwang, J et al. 2011). This increases the role of matrix material and fabrication process.

CNT+GNP/epoxy nanocomposites have shown an increase in piezoresistive response due to addition of second fillers which have potential for strain and damage sensing applications (Jiukun Li and Namilae 2016). In the next sections, development and testing of CNT+GNP/epoxy nanocomposites are explained and the improvements and comparison with the existing nanocomposites shall be highlighted.

2.2. Nanocomposite fabrication

Through several studies, CNTs in the form of buckypaper have shown great potential in fabrication of high performance nanocomposites. Due to its brittleness, buckypaper is usually infiltrated with epoxy to achieve the desirable strength and stiffness for strain sensing application (Jeffrey L. Bahr et al. 2001). In this study, neat epoxy resin,

modified with coarse graphene platelets (GNPs) are used with the CNT buckypaper to prepare the nanocomposites. Different epoxy resin matrices have been used to investigate the matrix with most desirable properties, these include.

- West system # 105 epoxy with #206 hardener

- Scotch weld 3M 2216 B/A gray epoxy

- Scotch Weld 3M 2116 B/A Translucent epoxy

The multiwall carbon nanotube sheet (buckypaper) consisting of 100% free standing nanotubes, with an area density of 21.7 g/m^2 and surface electrical resistivity of 1.5 Ω/m^2 is obtained from Nano Tech Labs. The coarse GNPs used as second filler were obtained by finely chopping conductive graphene sheet obtained from Graphene Supermarket. The surface resistivity of the graphene sheet is 2.8×10^{-2} Ω/m^2. The hybrid CNTs-GNPs nanocomposite specimen used for the mechanical testing are strips, 6.35 cm long and 1.27 cm wide cut from the buckypaper sheet with laser blade. Copper plates gauging 32, 1.27 cm long and 1.27 cm wide are attached at both ends of the strips to serve as electrodes using MG Silver epoxy, which has high adhesive and conductive properties.

Several strips are infiltrated with evenly mixed with resin-coarse GNPs of 5 wt. %. Previous experimental results indicate that the piezoresistivity in hybrid composites is higher for this combination of graphite platelets and CNTs (Jiukun Li and Namilae 2016). The resin nanocomposite is then cured at specified temperature and pressure based on the epoxy resin. The fabrication procedure is similar for all types of epoxy composites except for their curing parameters due to different epoxies. The comparison of composition and curing conditions of different epoxy matrices are given in Table 2.1. After curing, two wires are soldered, one to each copper plate. Figure 2.1 shows the different types of epoxy

nanocomposites prepared.

Table 2.1 Composition and curing conditions of different nanocomposites

Epoxy Matrix	Mix Ratio	Temperature	Pressure	Duration
West system # 105 epoxy with #206 hardener	5:1 (Epoxy to hardener)	Room temperature (25°C)	Vacuum pressure	12 hours
Scotch weld 3M 2216 B/A Translucent epoxy	1:1 (Part B/A) (by weight)	93°C (200°F)	Contact pressure	60 minutes
Scotch weld 3M 2216 B/A Gray epoxy	5:7 (Part B/A) (by weight)	93°C (200°F)	Contact pressure	30 minutes
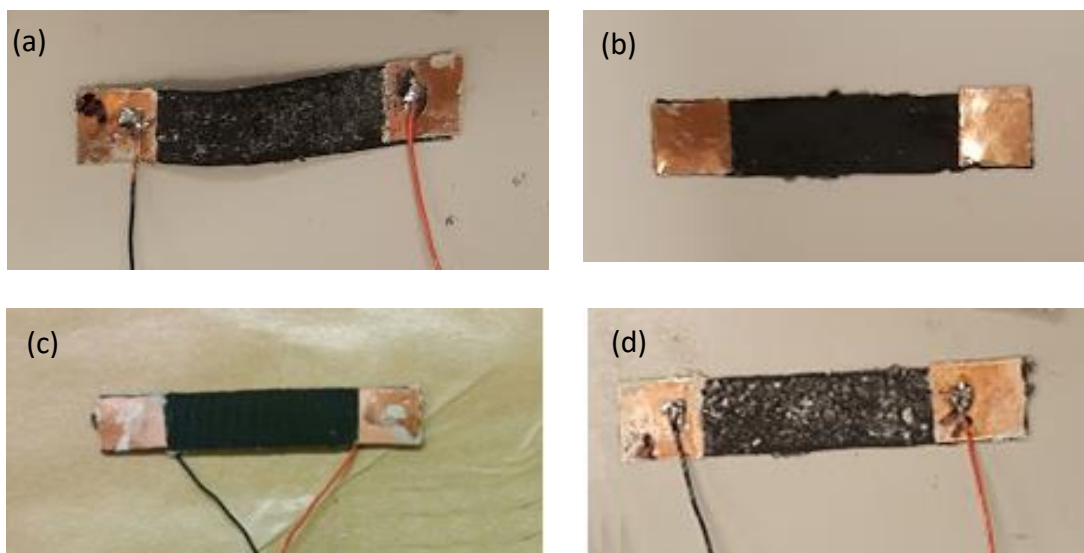
Figure 2.1 Different types of epoxy nanocomposittes (a) CNT+GNP/2216 Trans epoxy (b) CNT/2216 Gray epoxy (c) CNT+2216 Trans epoxy (d) CNT+GNP/2218 WS epoxy

2.3.   Surface Electron Microscopy

To measure the exact thicknesses of the specimen, Surface Electron Microscopy (SEM) has been used. SEM images of different samples are taken and discussed below.

2.3.1. CNT/2216 Translucent epoxy composite

Figure 2.2(a) shows the cross section area of only neat buckypaper cured with 3M Scotch Weld 2216 Translucent epoxy at 50x resolution. It is observed that the thickness of the specimen varies along the cross section, with wider cross section in the middle and thinner at the end. Possible reasons of this could be amount of epoxy infiltrated in the buckypaper and variation in the thickness of buckypaper itself. Figure 2.2(b) shows the thickness in the middle while Figure 2.2(c) shows the thickness variation near the edge at 150x resolutions. The average thickness of 95 micrometer is used for calculation purposes.
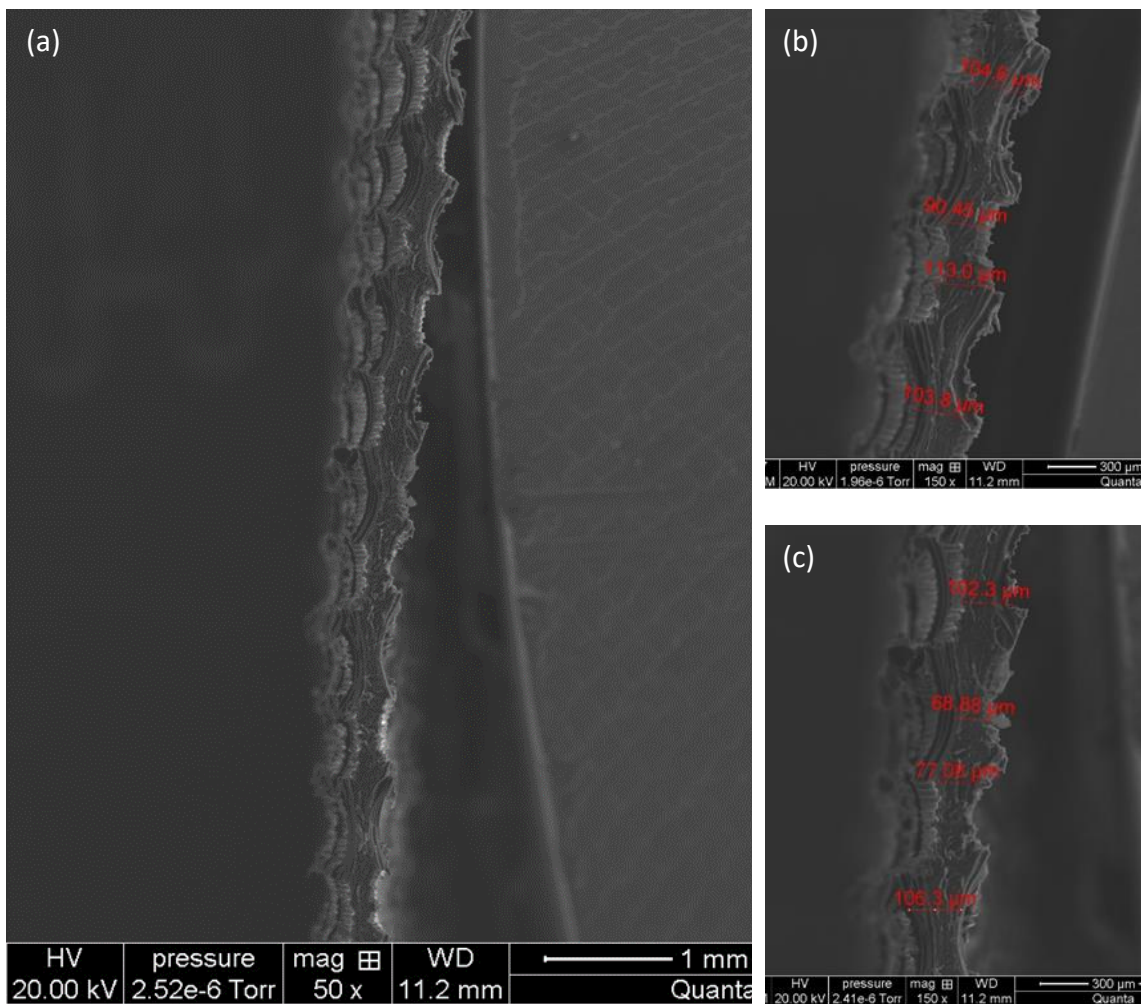
Figure 2.2. SEM Images of thickness of CNT/2216 Trans epoxy composite

2.3.2. CNT+GNP/2216 Translucent epoxy composite

Figure 2.3(a) shows the cross section area of neat buckypaper and graphene platelets (GNP) cured with 3M 2216 translucent epoxy at 50x resolution. Again, variation of thickness is observed as before, however the specimen with GNPs have larger cross section thicknesses as compared to neat buckypaper due to added graphene platelets. Figure 2.3(b) shows the thickness in the middle, while Figure 2.3(c) shows the thickness variation near the edge at 150x resolutions. The average thickness of 145 micrometer is used for calculation purposes.
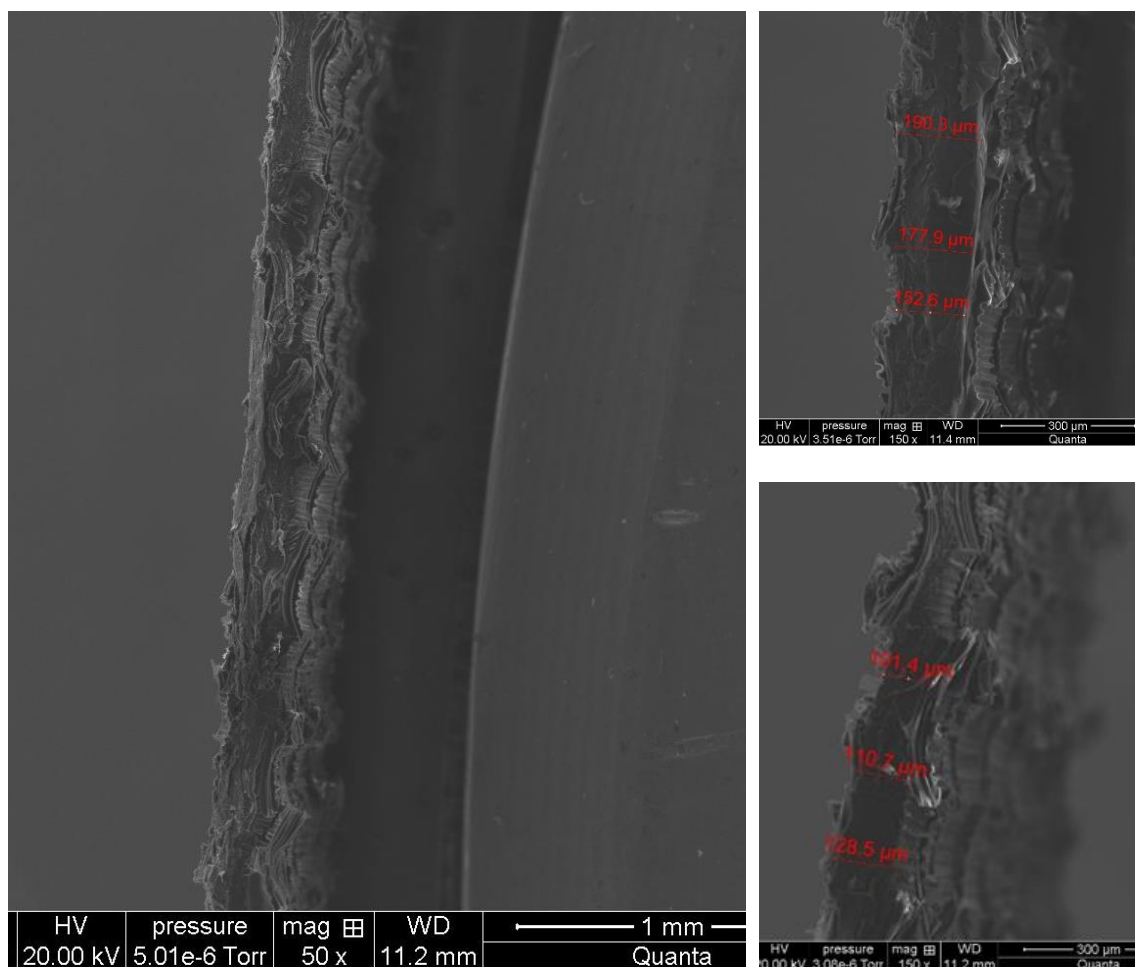
Figure 2.3. SEM Images of thickness of CNT+GNP/2216 Trans epoxy composite

2.3.3. CNT+GNP/West systems epoxy composite

Figure 2.4(a) shows the cross section area of neat buckypaper (CNT) and Graphene Nano-Platelets (GNP) cured with west systems 106 epoxy and 205 hardener at 50x resolution. Again, some variation in the thickness is observed. Figure 2.4(b) shows the thickness in the middle while Figure 2.4(c) shows the thickness variation near the edge at 150x resolutions. The average thickness of 1.65 micrometer is used for calculation purposes. The thicknesses found are somewhat different from similar reported epoxy composite in the literature (Jiukun Li and Namilae 2016) due to possible reasons for changes in buckypaper thickness and variations in manufacturing process.
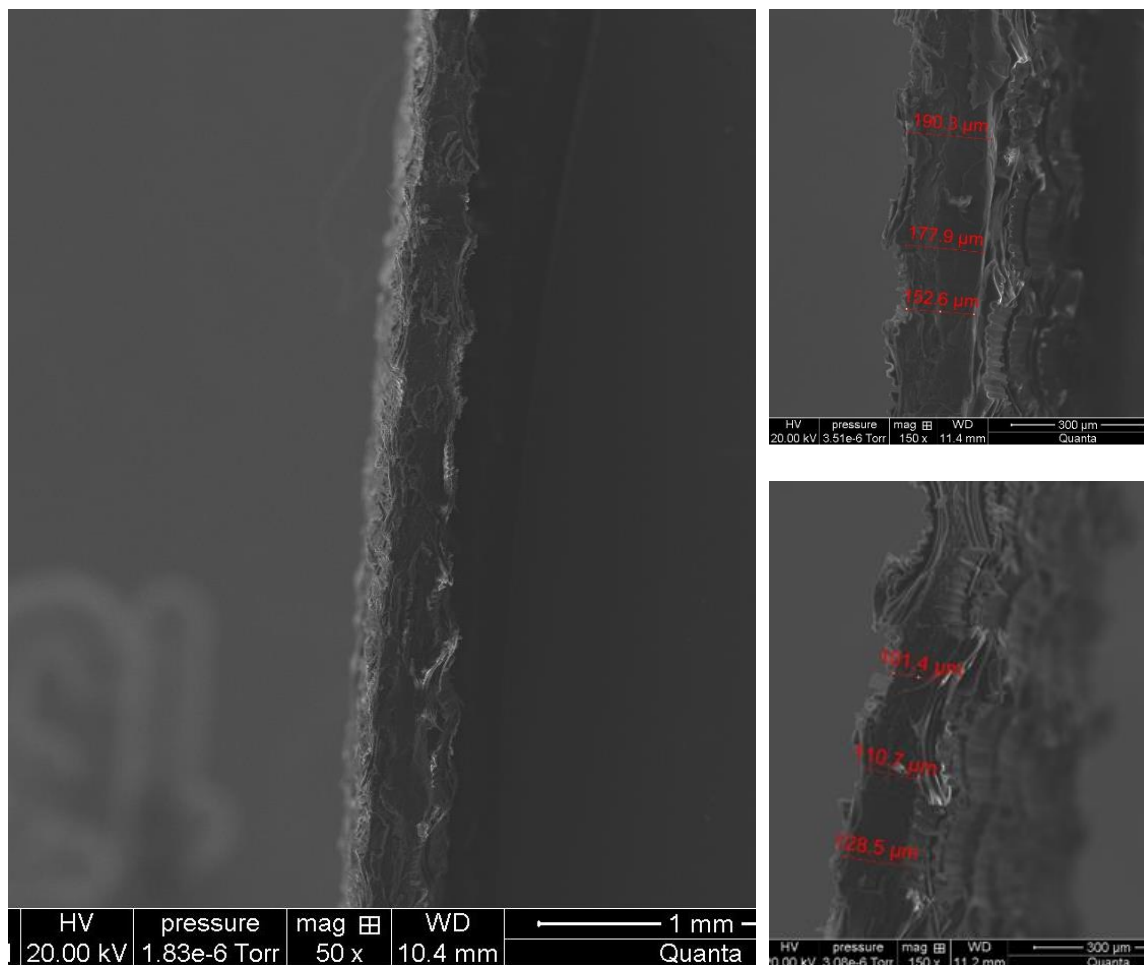
Figure 2.4. SEM Images of thickness of CNT+GNP/West systems epoxy composite

2.4. Tensile Testing

In order to investigate the mechanical and piezoelectric properties, tensile testing has been performed following IEEE and ASTM standard test methods (ASTM 2011) (ASTM 2012) (IEEE 2009). A four point probe testing method is used to measure the resistance of the hybrid CNTs-GNPs nanocomposites specimen before and during mechanical deformation. A constant intensity current of 0.1 Amperes is passed through the specimen and the resulting voltage drop is measured. Ohm's Law is then used to compute the specimen electrical resistance. In our study, a LabVIEW code is used along with a DAQ system to monitor the drop of voltage and to calculate the change in resistance before and during deformation. The static tensile test is conducted in the CS-225 Digital Force Tester at constant displacement speed of 0.167mm/sec. The test setup is shown in Figure 2.5.
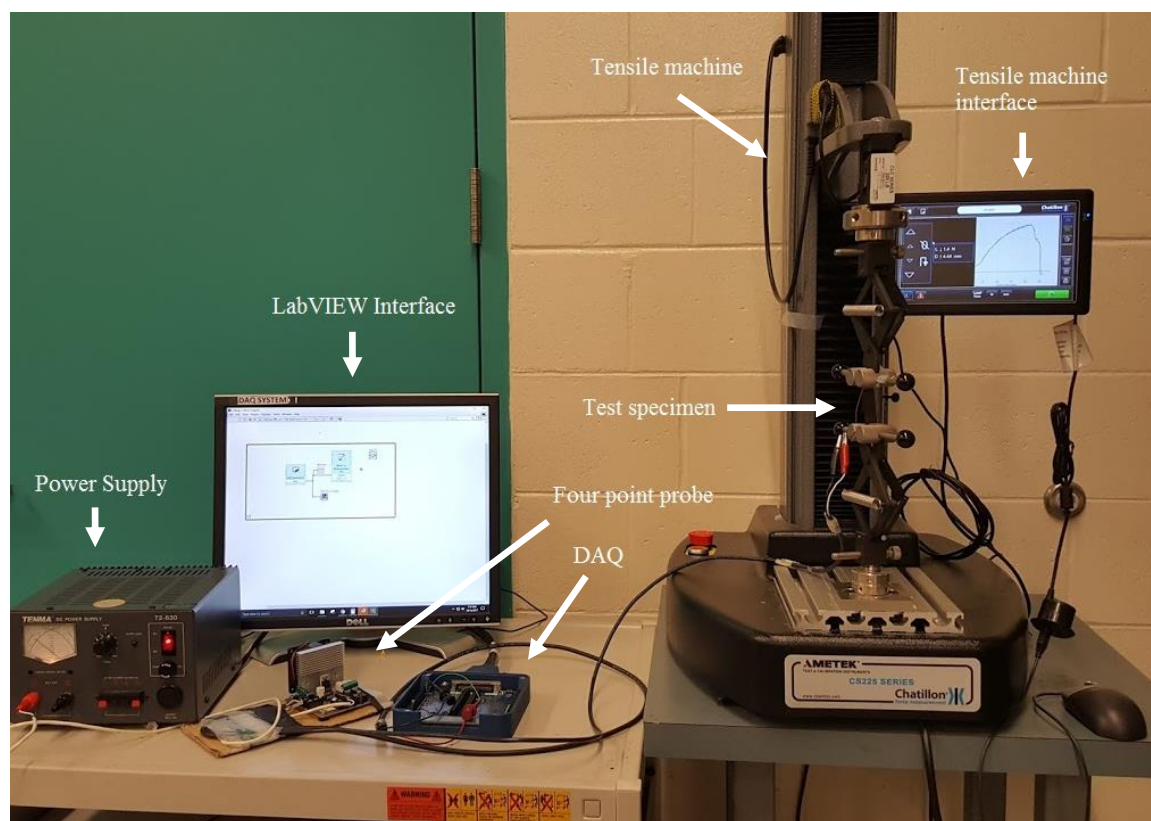
Figure 2.5. Test setup for tensile testing

2.4.1. Tensile test of CNT+GNP/2216 Translucent epoxy

The 2.5 in by 0.5 in nanocomposite sensors are prepared by adding 5% graphite platelets mixture with 3M 2216 B/A translucent epoxy. The stress stain curve is shown in Figure 2.6. It is also observed that the curve is less linear and the slope gradually decreases with strain. This is due to the viscoelastic behavior of the material which shall be discussed in Chapter 4 in detail. Assuming the curve as linear, the young modulus comes out to be 183 MPa.
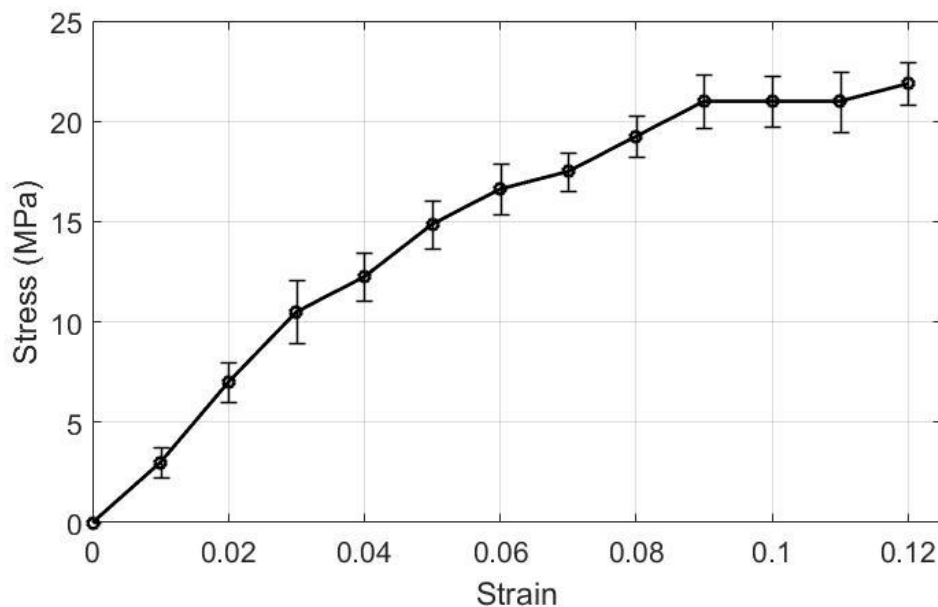
Figure 2.6. Stress strain response of CNT+GNP/2216 Trans epoxy composite

The electromechanical behavior of the nanocomposite is shown in Figure 2.7. It is observed that the electromechanical response with this epoxy is much higher. This is because the flexible matrix allows more expansion and hence change in piezoresistivity. The gauge factor is approximated to be around 10 for CNT+GNP/2216 Translucent epoxy composite.
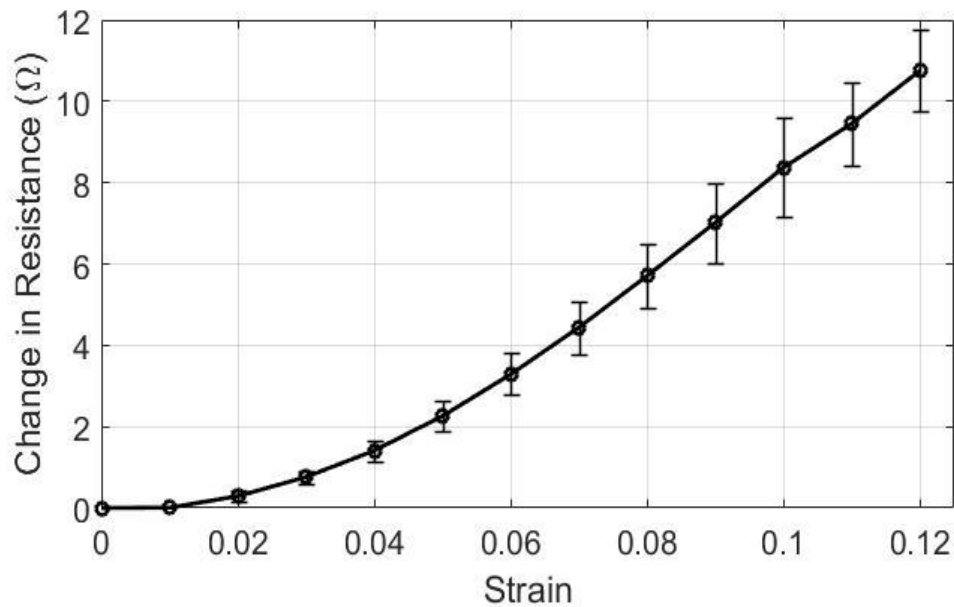
Figure 2.7. Change in resistance of CNT+GNP/2216 Trans epoxy composite with strain

2.4.2. Comparison of stiffness with different matrices in tensile loading

The comparison of mechanical tensile behavior of different types of nanocomposites is shown in Figure 2.8. It is evident that the nanocomposite with 3M 2216 translucent epoxy has much higher strains, i.e. more than twice, as compared to west systems epoxy. It can be seen that the maximum average strain before failure is 0.045% with mean failure stress around 20 MPa. The slope of the curve is high with the mean Young's modulus of 444.4 ± 10% MPa. Nanocomposites with 3M 2216 translucent and gray epoxies have relatively high value of ultimate strains going up to 12%. The slope of the nanocomposites with 3M epoxies is relatively less, with less variation among similar matrix materials. The average young modulus of nanocomposite with 5% GNP with 3M 2216 translucent epoxy is 175 ± 8% MPa which is quite less as compared to the CNT+GP/WS composite hence making it more flexible. Lesser stiffness is the indicative of more flexible material, which is desirable for its usage in inflatable structures. .
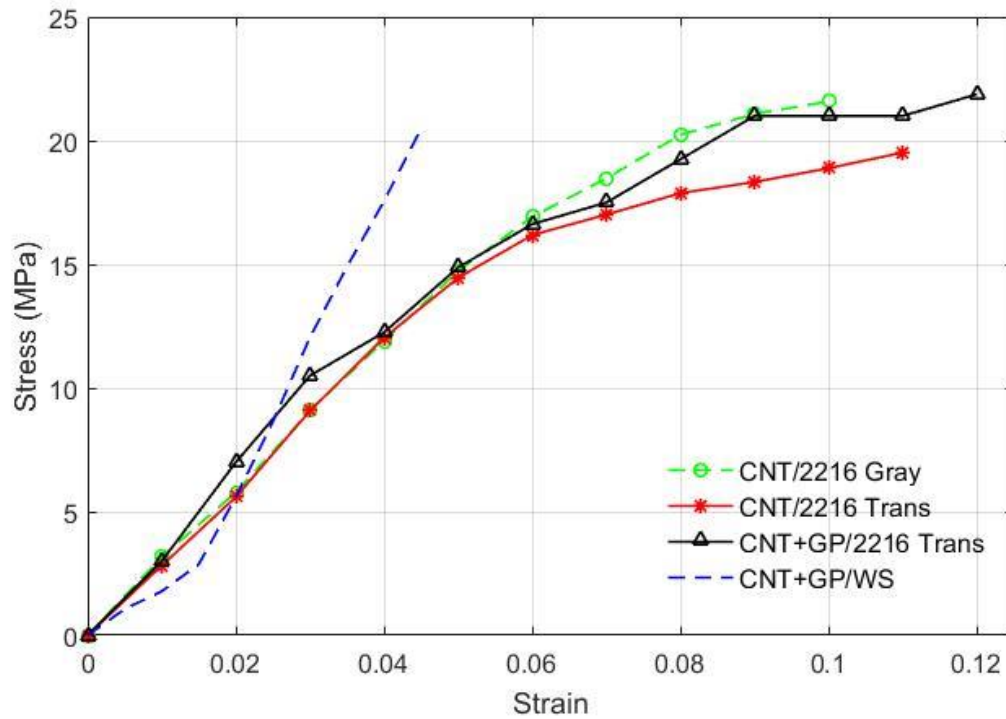
Figure 2.8. Comparison of stress strain behavior of CNT/2216 Gray, CNT/2216 translucent, CNT+GNP/2216 translucent and CNT+GNP/West systems epoxy nanocomposites

2.4.3. Comparison of electromechanical behavior with different matrices in tensile loading

The piezoresistive behavior of the nanocomposite with different types of matrixes is shown in Figure 2.9 and it is observed that all four types show similar piezoresistive trend. CNT+GP/WS shows a maximum change in resistance of 1.5Ω at maximum strain of 0.06%. CNT/2216 Gray and CNT/2216 Trans shows higher change in resistance with applied strains. When 5% GNPs are added into CNT/2216 Trans nanocomposite, the piezo-resistive response shows a definite increase. The maximum ΔR increases from 6.95Ω to 9.45Ω due to addition of second fillers.
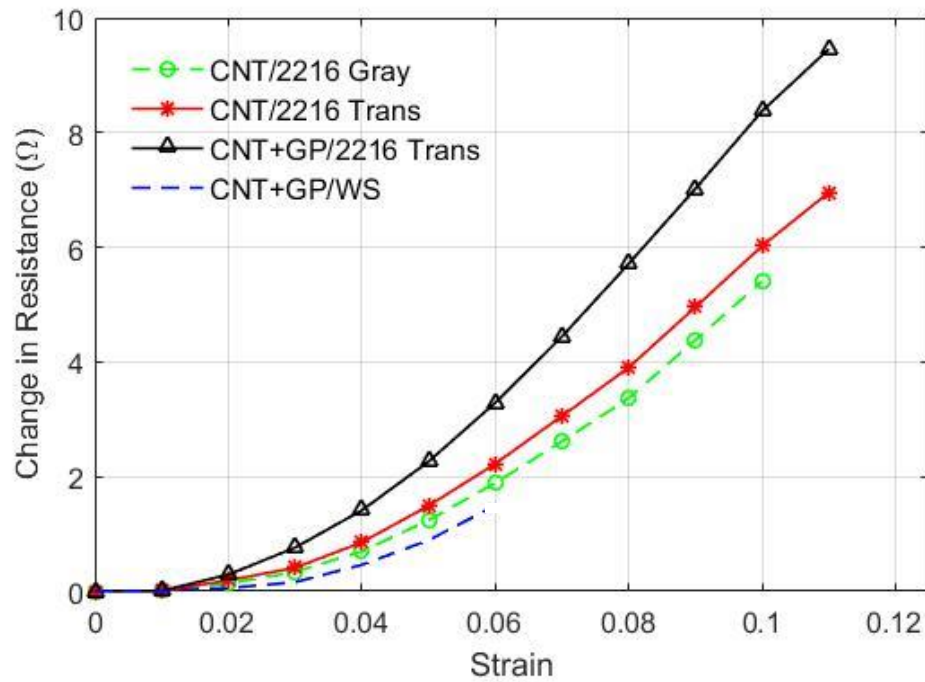
Figure 2.9. Comparison of resistance change with strain response of CNT/2216 Gray, CNT/2216 translucent, CNT+GNP/2216 translucent and CNT+GNP/West systems epoxy nanocomposites

2.5.   Strain variation within specimen during tensile testing

For the stress vs. strain plot and ΔR vs. strain plots, it is assumed that the strain variation is uniform throughout the specimen. Strain variation within the specimen is usually very less for uniform rigid specimen, however in this case there is strain variation within the specimen due to the flexible nature of the matrix material. To see the strain measurement within the specimen during the tensile test, Digital Image Correlation (DIC) technique is used. In this technique, strains are measured through non-contact method using optical technique. In this method, the gray and white speckles are created on the surface of the specimen. Due to strain, these speckles change their location with respect to each other, which are tracked and compared with the original (reference) image. This is shown in Figure 2.10. Based on movement of speckles, a correlation algorithm computes the shift in

each pixel of the image and provides an accurate strain map on the desired surface of the specimen.
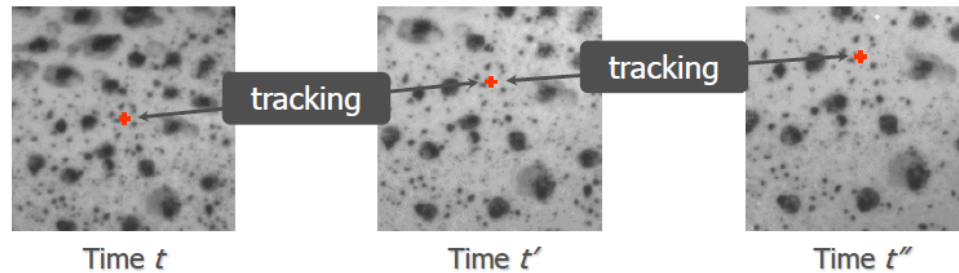
Figure 2.10. Tracking of speckles with time as the strain is applied (Correlated Solutions AN -708)

DIC systems can be either two-dimensional (2-D) and three-dimensional (3-D). In 2-D system, a single camera is placed parallel to the surface and 2-D displacements and strains are computed. However, 2-D DIC is limited only to planar specimens and can compute only in-plane strains. Any out-of-plane motion of the specimen will give erroneous results. However, in 3-D DIC system, two cameras are used to map the 3-D structure of the environment and this is called stereo-triangulation (shown in Figure 2.11). It involves computing the interaction of the two optical rays and requires calibration of the two cameras to formulate common coordinate system.
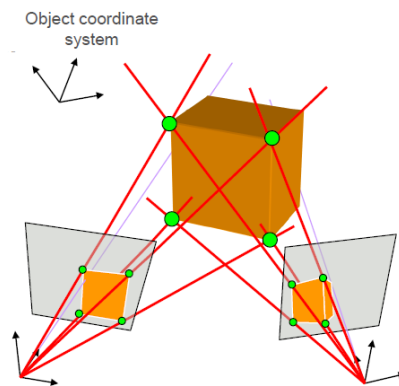
Figure 2.11. Stereo-triangulation for 3-D Digital Image Correlation (Reference manual Vic-3D 2010)

To compute the strain profile within the specimen during tensile test, VIC-3D system by Correlated Solutions is used. It consists of two 5 megapixel monochromatic cameras which have a maximum frame rate of 5 frames per second. The specimen needs to be speckled before the testing, to compute the strains through DIC. This is done by first coating the prepared nanocomposite specimen with a thin layer of white spray paint. Once it is dried, grey speckles are produced on the surface using Correlated Solutions speckle generator kit. Fine, high contrast, and random patterns are required to produce accurate strain results. This pattern can be seen on the speckled specimen as shown in Figure 2.12.

Figure 2.12. Speckled test specimen for digital image correlation

The test specimen is mounted in the tensile testing machine. The same procedure and equipment as mentioned before is used. Additionally, a light source is installed close to the specimen to provide good lightning conditions, which are essential for reliable DIC measurement. Two cameras at approximately 2 feet distance are mounted on the tripod stand facing the specimen for imaging. The cameras are calibrated using the calibrated grid before the test. The test setup shown in Figure 2.13.

The variation of strains within the specimen during the tensile test is shown in Figure 2.14. It is to be noted that the strain map of the specimen will vary with time, as the stress level is increased. DIC compare the strains with a refrence image, which in this case is the test specimen with zero strains without loading. Figure 2.14 shows the strain map of

the specimen prior to the rupture of the specimen. High strains shown in red color are seen

at the edge of the specimen and at the location of initiation of the crack. Figure 2.15 shows

the crack initiation on the middle left side of the specimen.
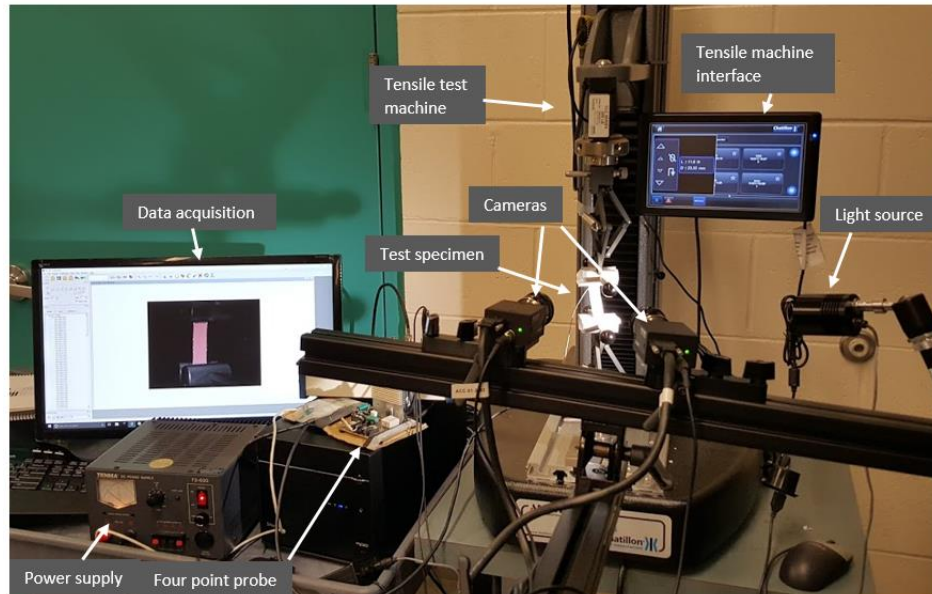
Figure 2.13. Test setup for strain measurement through DIC while tensile testing
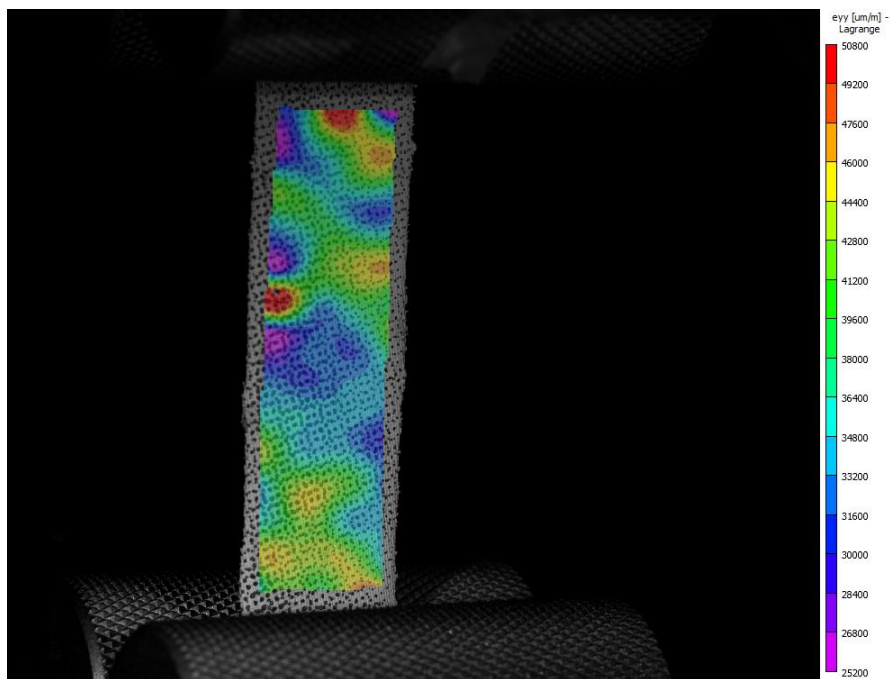
Figure 2.14. Strain variation with the specimen during tensile testing
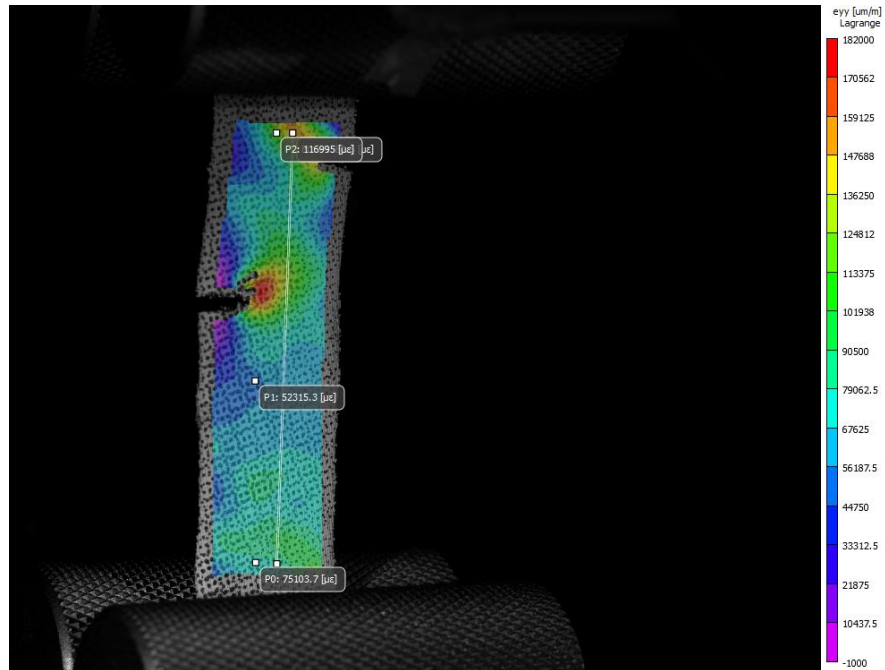
Figure 2.15. Crack propagation during the tensile test. 3 points and extensometer placed virtually on test specimen

Figure 2.16 shows the strain variation in the specimen when plotted against time. P0, P1, P2 are three different points picked on the specimen (shown in Figure 2.15) to show the variation in strain at different locations. Again these points are being computed from the zero strain position. Dash dotted line shows the average of the overall specimen and dashed line shows the virtual extensometer placed on the specimen. It is observed that strian is varied on the specimen and depending on location, strian can be higher or lower than the average strain as shown by P0 and P1, respectively. However the average strain value is almost same as the value obtained through virtual extensometer, which is used for calculation purposes.
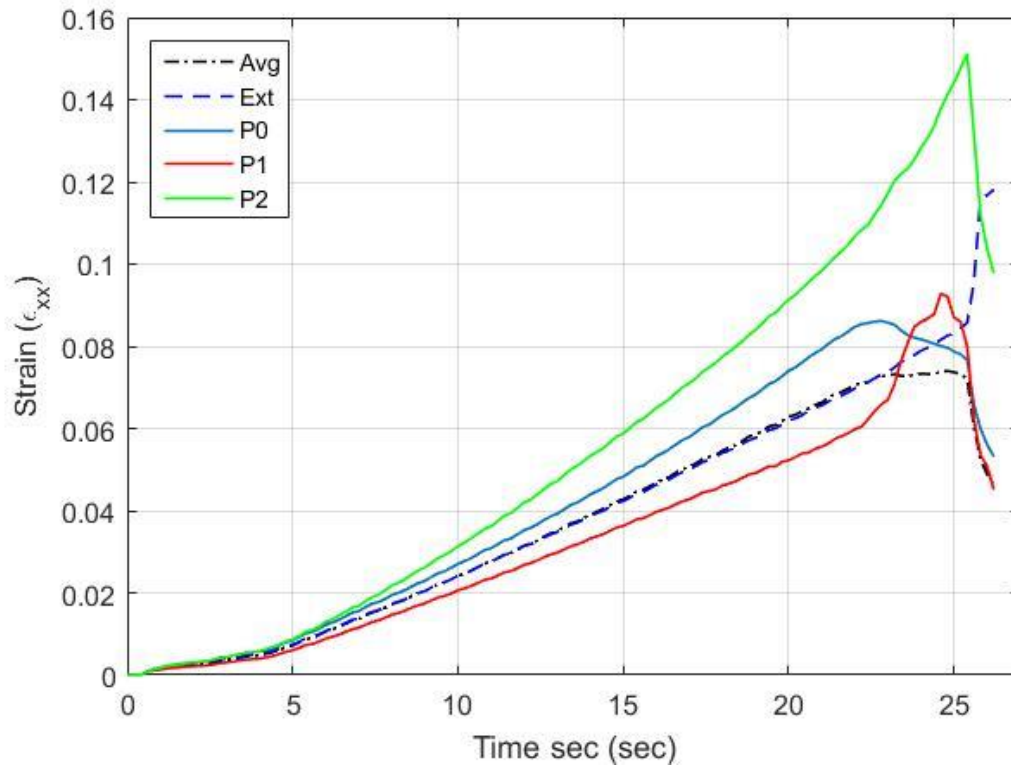
Figure 2.16. Plot showing strain variation of different points, average strains and extensometer strain w.r.t. time during tensile test.

The strain variation in the specimen occurs due to various reasons. For instance, as buckypaper is made of randomly oriented carbon nanotubes, local strains may vary based upon the various stiffness of randomly oriented CNTs. The variation in thickness of buckypaper itself and in the nanocomposite, as observed through the SEM, also vary the local stresses and hence changes in the strains. Moreover, non-homogeneity in the GNP/epoxy mixture due to graphite particles also causes slight change in mechanical properties and hence result in strain variation within the specimen.

3. Dynamic Testing

Mechanical vibrations are commonly found in most of the mechanical structures and especially in aerospace applications. The piezoresistive response CNT/epoxy and CNT+GNP/epoxy nanocomposites have been proven for static tensile loading. However, they dynamic response of the nanocomposites have not been fully investigated. In order to extend the capabilities of these sensors for measurement of vibrations, it is essential that the behavior should be investigated under cyclic loading. In this chapter, we discuss the testing of the CNT+GNP/epoxy nanocomposites under cyclic loading and study the effect of change in frequency, amplitude on the piezoresistive response. The response of different epoxy matrices on nanocomposite performance shall be investigated separately.

3.1. Literature Review

Few examples are found in the literature for electromechanical behavior of nanocomposites sensors under dynamic cyclic loading. Aldraihem et al. (Aldraihem, Akl, and Baz 2009) developed a functional paint sensor for vibration sensing by mixing urethane resin with Carbon Black (CB) nanoparticles. Dynamic response of the sensor was solved numerically and verified with experimental results, for a single oscillation frequency of 100 Hz. The applied amplitude displacement was approximately 2 µm, whereas the strains induced during cyclic loading were not mentioned. The sensors showed a good correlation between numerical and experimental results and response was much close to the applied loading.

Kang et al. (Kang et al. 2006) determined the dynamic response of 10% wt. single walled CNT (SWNT) sheet nanocomposite sensor with polymethylmethacrylate (PMMA) matrix. 3 mm × 5 mm specimen were mounted on cantilever beam which was allowed to

vibrate and damp naturally after an initial disturbance. The response of the sensor was identical to the laser displacement sensor for strain measurement.

In another study, response of polymer based 10% SWNT/PMMA strain sensors was also measured at low frequencies of 0.2 Hz to 5 Hz (Kang et al. 2006). Some other papers discuss the dynamic response of nanocomposite sensors with other fillers like ZnO (Kon et al. 2007) (Gullapalli et al. 2010) (Yin et al. 2011).

In subsequent sections, we characterize the piezo-resistive response of the nanocomposite under dynamic loading. Axial and transverse dynamic loading is applied in the range of low frequencies, i.e. 1 Hz to 50 Hz and the electrical response is measured. We study the effect of variation of both frequency and amplitude on the resistance change and see the strain variation within the specimen

3.2.   Experimental setup for dynamic testing

Figure 3.1 shows the schematic of test setup and Figure 3.2 shows the test setup itself. It consists of a vibration shaker, i.e. Modal Shaker 2025E by Modal shop, on which the CNT+GNP/WS epoxy nanocomposite is mounted. One end of the nanocomposite sensor is horizontally connected to the shaker with its other end fixed with clamps. The shaker is controlled by a computer via an amplifier and a vibration input module. An accelerometer is also mounted on the shaker to measure the force generated. Polytec OFV-505 laser vibrometer sensor is used for measuring the exact displacements induced by the shaker. The two electrical wires connected to the electrodes of the specimen are connected to another current source (set to 0.1 A) and a data acquisition system (DAQ) using four-point probe to measure the voltage change through the nanocomposites strip. In this test setup, it is assumed that all the displacement induced by the shaker is directly translated to

the specimen and there is no initial bending in the specimen.
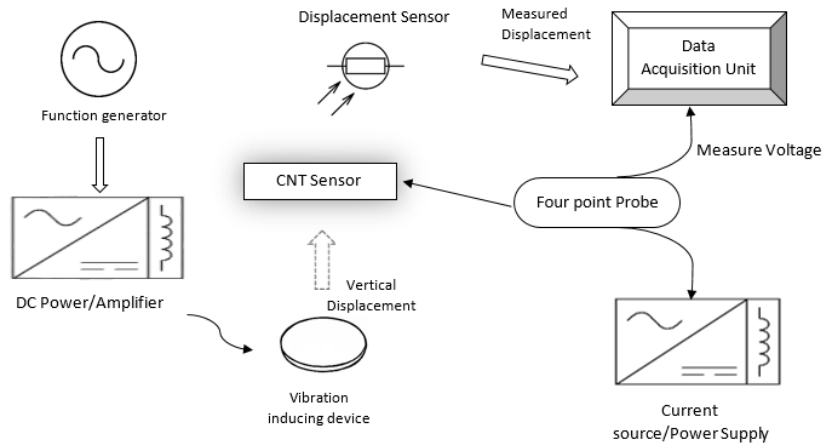
Figure 3.1 Schematic for test setup for vibration testing
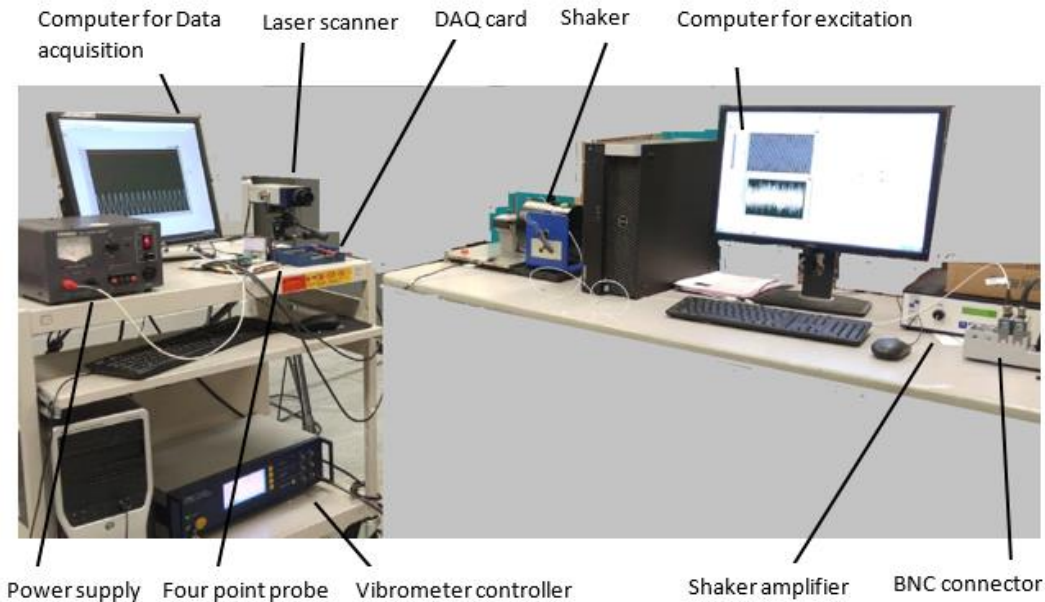
Figure 3.2. Experimental setup for axial dynamic testing

This test setup is used to characterize the piezo-resistive response of the nanocomposite under axial vibrations. Axial dynamic loading is applied under low frequencies, i.e. 1 Hz to 50 Hz with displacement amplitude ranging from 0.2 to 1.2 mm, while the resistance of the nanocomposite is simultaneously measured using four point

probe. Effect of the variation of both frequency (at constant displacement amplitude) and displacement amplitude (at constant frequency) on the change in resistance is measured and analyzed.
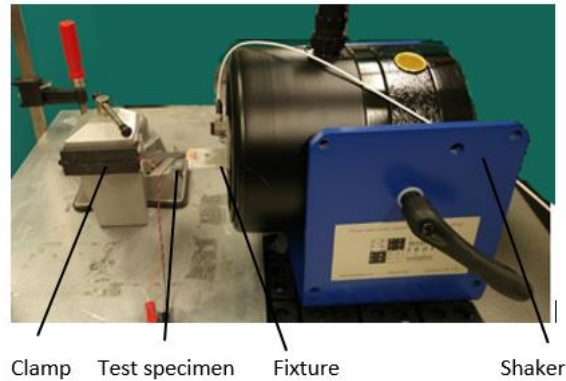
Figure 3.3. A closer look on the mounting of sensor with the clamp and shaker.

3.3. Effect of cyclic loading on electromechanical response

In this section, the piezoresistive behavior of the sensor under axial dynamic loading is examined. Frequency values in the range of 1 Hz to 50 Hz are used for the vibration of the specimen. Figure 3-4 and Figure 3-5 show the resistance change ratio of the sensor for frequency values of 5 Hz and 50 Hz respectively, with a peak axial displacement of 1.2 mm.
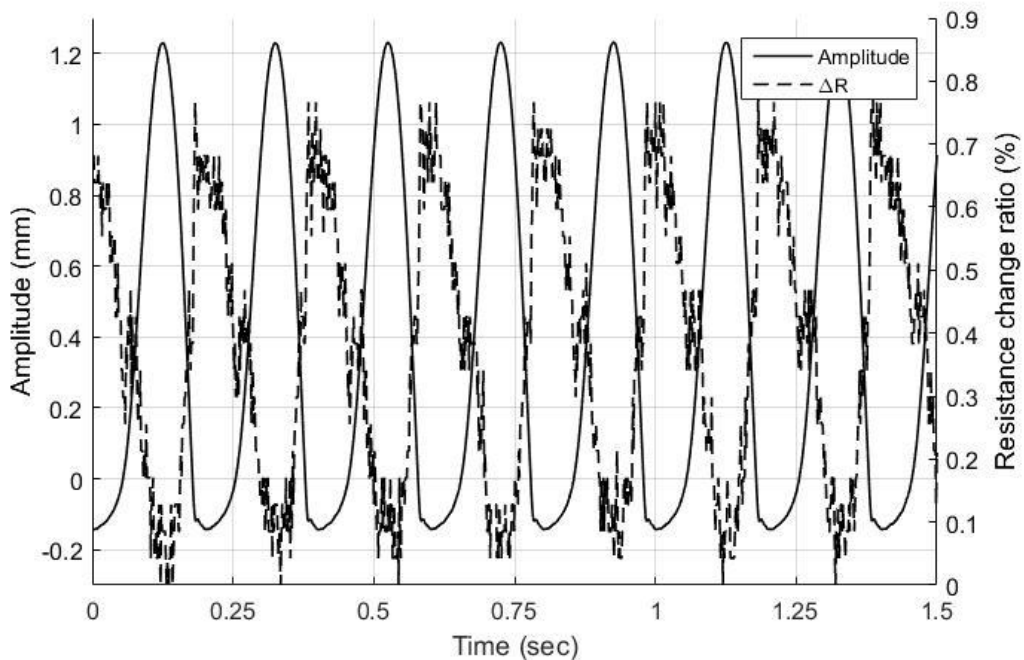
Figure 3.4 Variation of amplitude of vibration and resistance change with time at 5 Hz
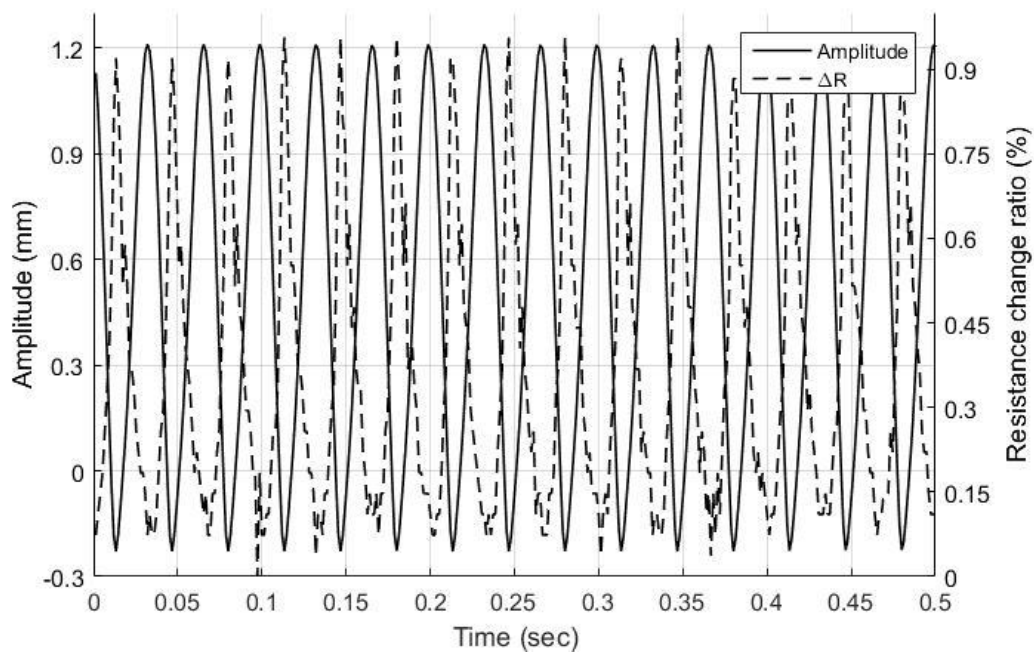
Figure 3.5 Variation of amplitude of vibration and resistance change with time at 30 Hz

The displacement amplitude is kept constant for each of the frequencies. As seen

from the plots, the resistance curve of the nanocomposite sensors follows the induced axial

strain for both low and high frequencies. This shows that the resistance change in the specimen varies in the same way as the excitation displacements and the specimen can catch the excitation frequencies. At the same amplitude, we note that the nanocomposite exhibits smaller resistance change at the lower frequency (5 Hz) compared to higher frequency (50 Hz). Overall, Figure 3.4 and Figure 3.5 show that the sensor retains its piezoresistive behavior under axial dynamic loading and exhibits repeatable and consistent change in resistance during each cycle in the range of 1 Hz to 50 Hz.

3.4.   Effect of excitation frequency on electromechanical response

Figure 3.6 shows the variation of resistance change ratio with respect to frequency while the displacement amplitude is kept constant at 1.2 mm. Error bars show the variation in readings for multiple tests. It can be seen from the graph that is some increase in piezoresistivity happens for frequencies ranging from 1 to 10 Hz. After 10 Hz there is no significant change in the resistance.
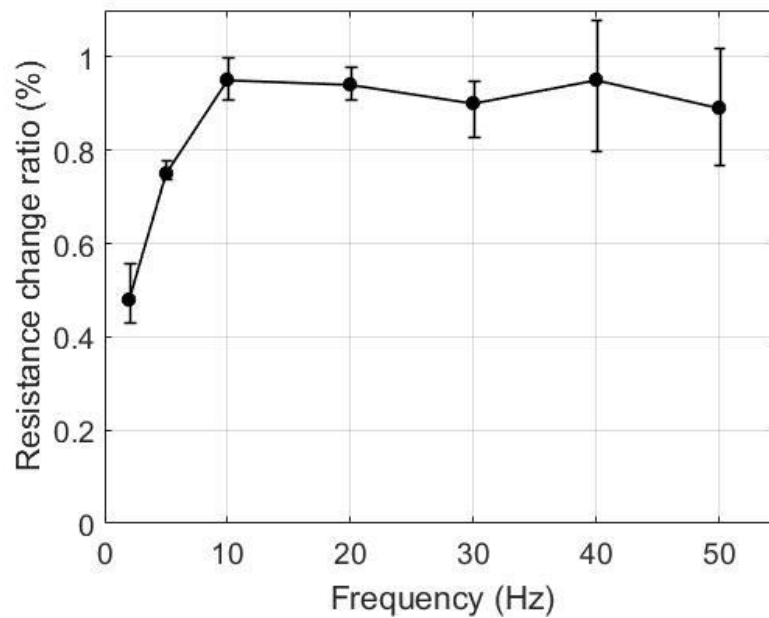
Figure 3.6. Effect of change frequency on resistance change ratio

3.5. Effect of amplitude on electromechanical performance

Figure 3.7 shows the change in resistance due to a change in displacement amplitude with the frequency kept constant. Frequencies values of 10, 30 and 50 Hz were examined in that test condition. We see a clear increase of the sensor piezoresistivity with an increase of the displacement amplitude for all the values of frequency studied. This is expected because increased amplitude correlates with higher induced strains, which corresponds to the behavior similar to static tensile test. Hence it is seen the piezo-resistive performance of the nanocomposite is similar in dynamic testing as compared to static tensile testing.
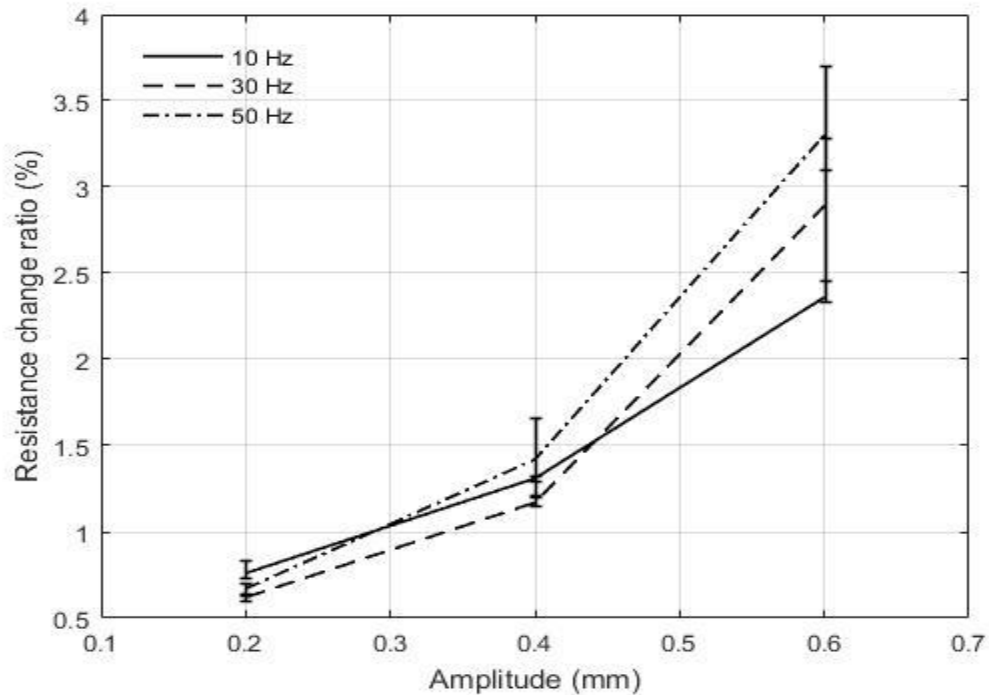
Figure 3.7 Effect of change in amplitude on resistance change ratio

3.6. Strain variation within the specimen during vibration testing

The variation in amplitude of vibration has been associated with the response of the nanocomposite; however, it would be more insightful to see the strain variation within the specimen and how it varies during the cycle. For this purpose, DIC is setup along with the shaker setup. The CNT+GNP/2216 Translucent epoxy specimen is speckled and mounted in same fixed free condition as before and cameras are mounted at the top along with appropriate lightning conditions to obtain good quality images. The test setup is shown in Figure 3.8.

Computer for excitation and data acquisiton — Cameras — Shaker — Test specimen — Light
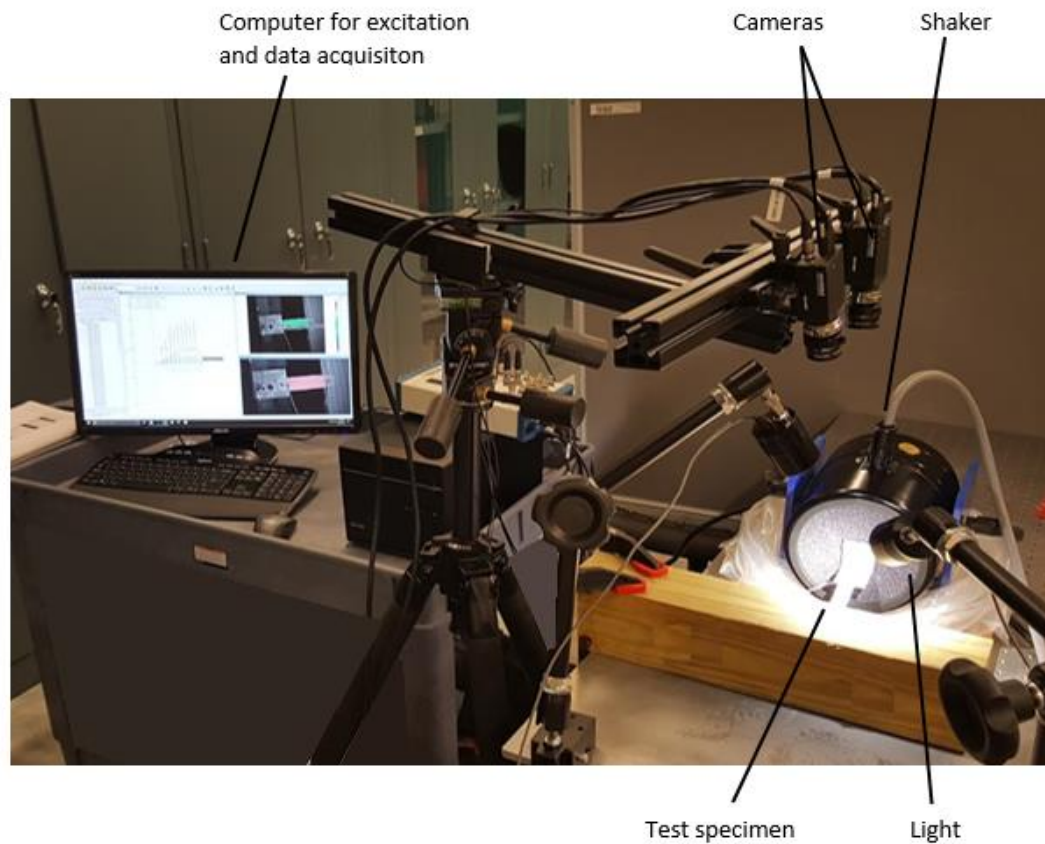
Figure 3.8 Test setup for strain measurement through DIC while vibration testing

During vibrations, the deformation varies within the cycle and DIC would require to take sufficient images in each cycle to develop the strain profile. This would bring the camera frame rate into consideration and a lower frame rate camera would not be able to capture a frequency that is equal to or higher to it. To encounter this issue, the DIC measurement system is connected with the vibration input signal to get information of time, frequency and phase of the vibration signal. DIC software then triggers the cameras once, after specific number of cycles and sweeps the phase over imaging time to get image of full cycle. This can be understood from Figure 3.9. For example, for 10 Hz sine signal, the cameras would be triggered at 0° phase in the first cycle and at 30° phase in the second cycle, and in this way it will capture one full sine wave in total of 12 cycles. Therefore

during a single test, it is important to keep the amplitude and frequency constant over time

in   order   to   get   similar   values   of   strains   with   time.
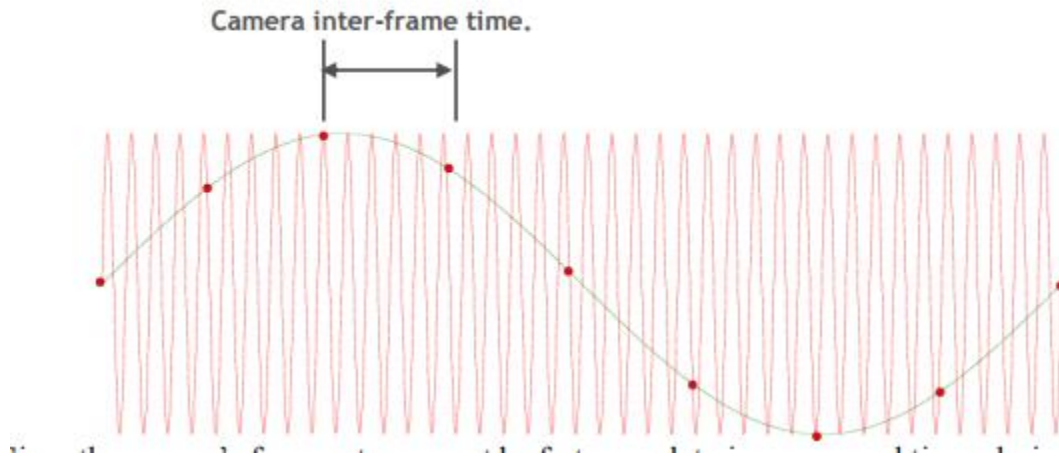
Figure 3.9. Camera triggering in DIC to capture full cycle during vibration (Correlated Solutions AN -708)

Figure 3.10 shows the test specimen at 5 Hz at reference position, i.e. without application of any loading. Four points are picked across the specimen, two at each ends, two randomly in the middle and an extensometer is placed across the specimen. Figure 3.11 shows the variation of strains at these points in x-direction i.e. the longitudinal direction of the specimen, when the shaker is excited with since wave of frequency 5 Hz.
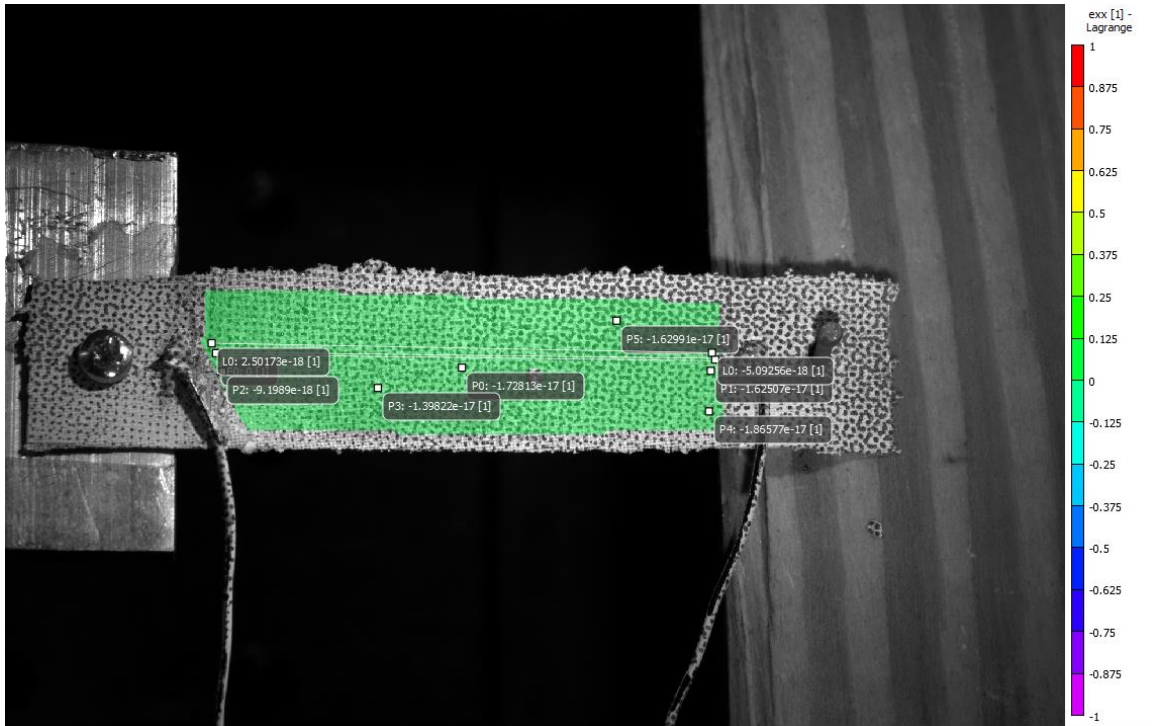
Figure 3.10. Reference image at zero strain condition and position of points on the specimen at different locations

It can be seen that all the points follow the applied sine wave loading on the specimen, however the strains vary significantly at different points. Point P0 which is at the free end of the specimen, shows the highest strain which is more than the average strain of the specimen. Point P3 which is somewhere in the middle shows the least amount of strain. Dashed line shows the strain variation of the extensometer placed across the specimen which is almost same as the average strain. Two x-axes are plotted in Figure 3.10. One axis shows the DIC time stamp, i.e. the time over which the DIC took images to capture the whole plot. Second axis shows the time in seconds which represents the time of the wave according to its frequency. The plot shows 5 complete cycles in 1 second which represents a 5 Hz signal, i.e. the applied excitation signal. However, since DIC took the images with 30° phase shift, it captured images of 1 cycle in 12 actual cycles and it took 60 cycles to capture 5 cycles of strain measurement. Therefore, the DIC time stamp shows
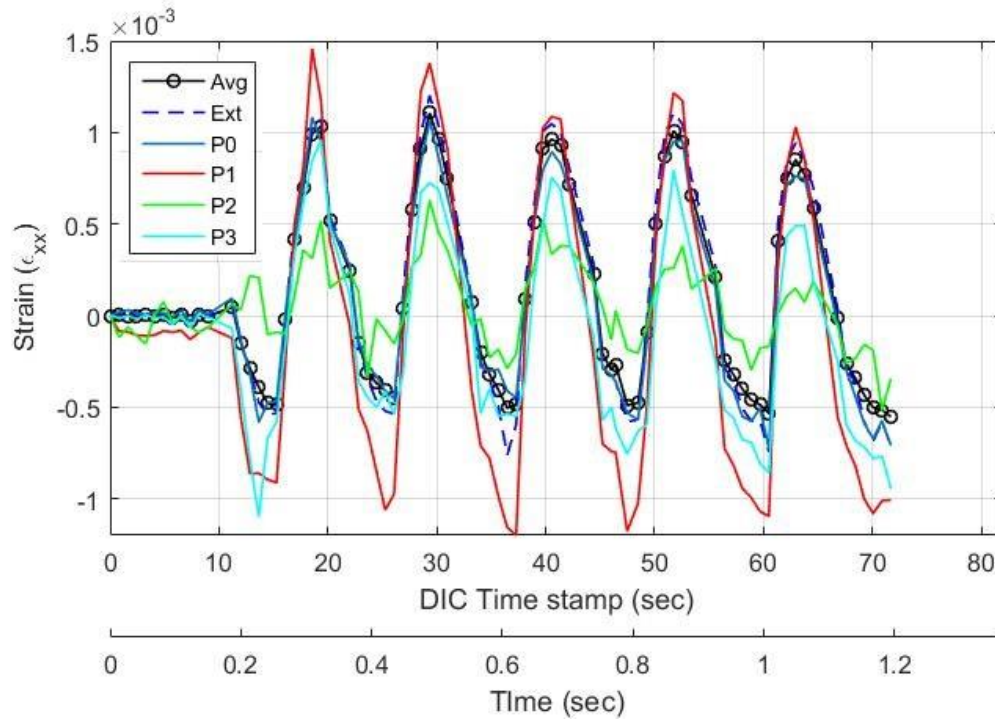
Figure 3.11. Variation of strain at different points on the specimen at 5 Hz frequency.

that it took 60 seconds in total to show the strain plot shown in Figure 3.11.

Figure 3.12 shows the strain map of the specimen when it is in maximum tension, i.e. at 90° phase angle while Figure 3.13 shows the strain variation at maximum compression i.e. when it is at 270° phase angle. The two figures should not be compared with each other as they both have different strain scale, which is in order to show variation within the specimen properly in each figure. If the same scale would have been chosen, Figure 3.13 would have been all in purple and blue shade, due to overall lesser strains.

Figure 3.12. Strain map of the specimen at the maximum tension

Figure 3.13. Strain map of the specimen at maximum compression

Another useful feature that is obtained from DIC is plot of line slices (shown in Figure 3.14) where a line drawn in the middle of the specimen across its length is analyzed over a complete vibration cycle. Y-axis shows the strain in the axial direction while x-axis

is the position in x-axis along the line from left to right of the specimen. Different lines shows the shape of the line of in other words, shape of the specimen at different intervals. The thick red line at the bottom shows the shape of the line when the specimen is at 270^0 phase or in maximum compression. The thick blue line at the top shows the shape of the line when the specimen is in maximum tension or 90° phase position. It can be seen that strain goes negative when the specimen is in compression, and positive when in tension. Moreover, positive and negative strains have larger values towards the right side of the specimen which can also be confirmed from strain variation maps in Figure 3.12 and Figure 3.13. It is also noted that the specimen does not necessarily forms a sinusoidal shape along the excitation cycle which can be seen from the shape of the line curves in Figure 3.14 as well.
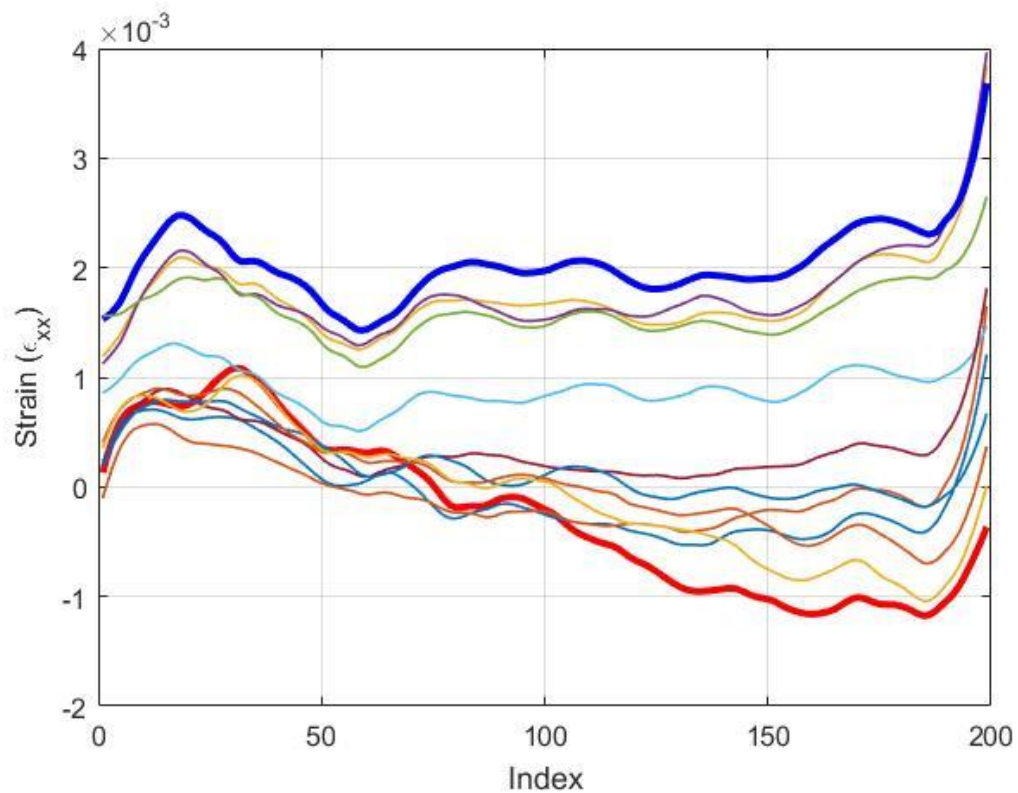
Figure 3.14. Line slices showing the variation of specimen cross section and strains over the cycle

3.7. Resistance change w.r.t. average strain in dynamic loading

Figure 3.15 shows the variation in resistance change with strain in the CNT+GNP/2216 Trans epoxy composite specimen at various frequencies. Since the strain varies from point to point in the specimen, average strain values have been used for computation. It shows that in dynamic loading the resistance change increases at higher strains as expected. This confirms with the previous results of increase in piezoresistivity with increase in amplitude in dynamic testing and the response is identical to static tensile testing. The trend is same for different frequencies; however, there is slight variation in the ΔR values at different frequencies. The data is limited to few samples, therefore, it is expected that with large number of samples, the variation will lie within the error bars.
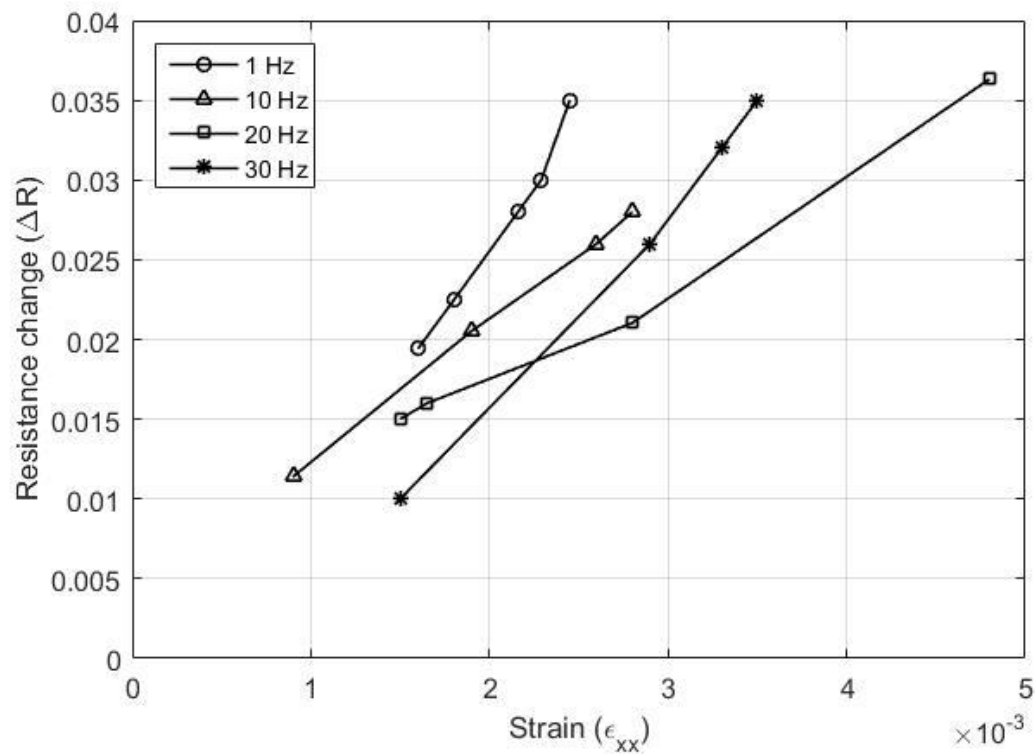
Figure 3.15 Change in resistance change with strain at different frequenices

4. Dynamic Mechanical Analysis

4.1   Introduction

Dynamic mechanical analysis (DMA) also called as Dynamic Mechanical Spectroscopy (DMS) or Dynamic Mechanical Thermal Analysis (DMTA) is used to understand and characterize the viscoelastic behavior of materials, more commonly polymers. Viscoelasticity is the property of materials that show both elastic and viscous behavior while undergoing mechanical deformation. In pure elastic materials, the strain rates are not dependent on time, whereas in viscoelastic materials, strains not only depend on applied force, but at the strain rate as well. This is also accompanied with the energy dissipation on application of loads, which leads to hysteresis. So instead of s typical stress strain curve, there is a hysteresis loop in a stress/strain plot of viscoelastic material exhibiting the energy loss involved in the process. This is shown in Figure 4.1.

(a)   (b)
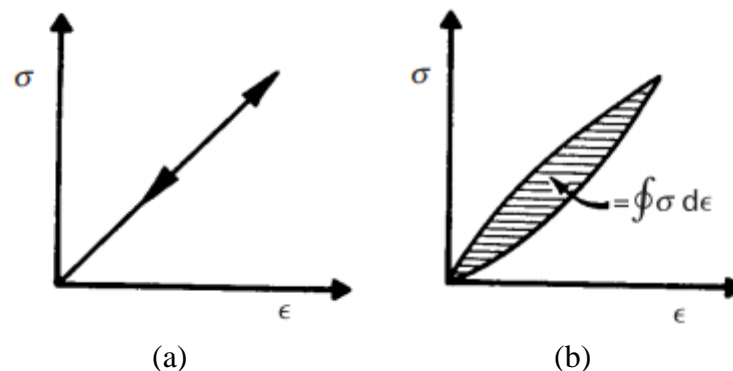
Figure 4.1 Stress-strain relation of (a) elastic materials, (b) viscoelastic materials.
(Meyers and Chawla e2009)

In dynamic mechanical analysis, visco-elastic behaviour of the material is observed by applying small deformation in a repetitive manner and the response of the material to stress, temperature, frequency and other paratmers is observed. DMA measures stiffness and damping of the material in terms of modulus and tan delta ($\tan \delta$). Modulus can be

expressed as storage modulus, or loss modulus. Storage modulus, (E') is the measure of energy stored or elastic solid like behaviour of the material. Storage modulus is not exactly the stiffness of the material as DMA accounts for geometry factor aswell. Loss modulus (E'') is the measure of energy disspitated as heat and represents the viscous behaviour of the material. Storage and loss moduli can also be described as in-phase and out-of-phase components of the force displacement curve as the sinusoidal force is applied. For an applied force at a frequency ω, the strain is out of phase by the phase angle δ, dynamic stress σ and strain ε can be expressed as

$$\sigma = \sigma_o \sin(\omega t + \delta)$$

$$\varepsilon = \varepsilon_o \sin(\omega t)$$

Dynamic stress can be further expressed as in-phase and out-of-phase components as

$$\sigma = \sigma_o \sin(\omega t) \cos\delta + \sigma_o \cos(\omega t) \sin\delta$$

Expressing in terms of strain and using E' and E'' for in phase (real) and out of phase (imaginary) parts, complex modulus E^* can be expressed as

$$E^* = \frac{\sigma}{\varepsilon} = \frac{\sigma_o}{\varepsilon_o} e^{i\delta} = \frac{\sigma_o}{\varepsilon_o}(\cos\delta + i\sin\delta) = E' + E''$$

This infers that storage and loss moduli are real and imaginary part of complex modulus. Tan delta is the ratio of loss modulus to storage modulus and is often called as damping ratio. It give the measure of enegy dissipated by the material.

$$\tan\delta = \frac{Storage\ Modulus}{Loss\ Modulus} = \frac{E'}{E''}$$

With an increase in temperature, the material transforms from elastic glassy state to soft rubbery state. The temperature at which this occurs is called glass transition temperature (T_g). Storage and loss moduli are temperature and frequency dependent

properties and their variation with these parameters is an important characteristic obtained from DMA.

4.2   Literature Review

Since the CNT based nanocomposites are made of epoxy matrix, the mechanical properties of the matrix are likely to change with variation of temperature and frequency. It can effect on the electro-mechanical performance of the nanocomposite as well, therefore, dynamic mechanical analysis is required to investigate this behavior. Composites with several different types of epoxy/polymer matrix and SWNT/MWNT fillers have been developed and tested in the existing literature. A few of these nanocomposites and their DMA results are discussed below.

The behavior of carbon nanotube polyvinyl alcohol $[CH_2CH(OH)]_n(PVOH]$ composites under thermo-gravimetric analysis (TGA) and DMA was investigated by Shaffer et al. (Shaffer and Windle 1999). Modulus showed a drop around 60 ℃ for all weight fractions, i.e. from 10 wt% to 60 wt% and similarly an increase in tan delta at the same temperature. This shows the T_g value of the composite around 60℃.

Carbon nanotubes (CNTs) and methyl-ethyl methacrylate (MEMA) copolymer composites with nonionic surfactant (triton X-100 t-octyphenoxypoly-ethoxyethanol) and the plasticizer (trytolyl phosphate) have shown significant decrease in storage modulus with increase in temperature for all concentrations. The T_g values as found from DMA testing varied between 88 ℃ and 102 ℃ for various concentrations of MEMA and surfactants. The results obtained through differential scanning calorimetry (DSC) showed slightly higher values of T_g for same concentrations (Velasco-Santos et al. 2003).

Nanocomposites based on atactic polypropylene (aPP) and MWNTs shows increase in storage modulus and broad tan delta peaks with increase in MWNT content. T_g value varies between -20℃ and -10℃ for pure aPP and 5% aPP/MWNT composite. Li et al. (X. Li et al. 2004) studied nanomechanical and viscoelastic properties using nano-indentation DMA tests. Storage modulus showed slight decrease while loss modulus showed some increase with increase in frequency up to 100 Hz.

MWNTs dispersed in thermosetting phenylethynyl terminated polyimide Triple a PI (TriA-PI) showed a high glass transition temperature, i.e. T_g > 300 ℃ due to its matrix. A negligible effect of MWNT content even at higher concentrations i.e. up to 14.3%, on elastic modulus and glass transition is observed. This is due to predominant effect of the TriA-PI matrix. Similarly CNT did not had an effect on T_g with polyether ether ketone (PEEK) composites (Ogasawara et al. 2004).

Bisphenol A diglycidyl ether (DGEBA) epoxy and Ruetapox LV 0164 resin with poly-etheramine hardener were mixed with non-functionalized and functionalized MWNTs to develop epoxy composites by Gojny et al. (Gojny and Schulte 2004). Storage modulus and tan delta curves show that increase in MWNTs to epoxy resin did not have any effect on storage modulus in glassy region, however in rubbery region, a significant increase was observed. Functionalized nanotubes had a distinctive increase in glass transition temperature. T_g values were found in the range of 65 ℃ and 85 ℃ for functionalized as well as non-functionalized nanotubes.

Dynamic mechanical analysis of polycarbonate (PC)/MWNTs composites showed that with increase in weight fraction of MWNT, dynamic modulus and viscosity of the

nanocomposite increased. Frequency dependence is observed for storage modulus as well as tan delta. With increase in frequency, storage modulus increase up to frequency of 100 Hz for all concentrations. Trends of tan delta were different for lower and higher concentrations but an overall increase is observed with the increase in frequency (Abdel-Goad and Pötschke 2005). In another study, (Sung et al. 2005) DMA of PC/MWNT composite showed drop in storage modulus and tan delta peak around 150℃ for all different composition fractions of PC/MWNT (85/15 to 100/0). After annealing the samples at 190℃ for 8 hours, tan delta peaks were shifted towards higher temperatures and the peak values were significantly lowered. It was concluded that for lower content of MWNTs behavior of PC is determining the T_g values. At higher contents and after annealing, MWNT confines the PC chains resulting in shift in tan delta peaks.

Rajoria et. al. (Rajoria and Jalili 2005) investigated stiffness and damping properties of both SWNTs and MWNTs carbon nanotube-epoxy composites of different concentrations. The trends shown for storage modulus in frequency scan is very irregular and does not shows any trend. Loss modulus showed increase with frequency up to 200 Hz but the trend was not very clear.

DMA of pure natural rubber (NR) and MWNTs composite reveals the glass transition temperature at quite low temperature of -60℃. Increase in MWNT content resulted in significant decrease in peak values of tan delta, however it did not alter the T_g value. For polymethyl methacrylate (PMMA) and unmodified SWNTs composites, tan delta peak occurs around 105℃ for pure polymer and T_g increases by 30℃ with addition of SWNTs (Bokobza 2007).

SWNT also had a reinforcing effect on composites made from SWNT and isotactic polypropylene (iPP) but till a maximum percentage of 0.75%. Increase in SWNT content had an increase in storage modulus, but did not cause much variation in glass transition temperature. The peak of T_g curve occurred around 0℃ for for all concentrations from 0-1% of SWNT contents (Manchado et al. 2005).

Polyurethane/MWNT composites with 2 wt % MWNT content were prepared and characterized by Xiong et. al. (Xiong et al. 2006). Increase in T_g from -5.4 ℃ to 6.2℃ was observed from the composite. MWNTs had an increased effect on storage modulus below the T_g, but no affect above T_g value. In another study (Xia and Song 2005) introduction of SWNT in PU had a slight decrease in T_g and damping capacity. The glass transition temperature was found to be between -50℃ and -40℃ for 0% to 2% wt% of SWNT/PU composite.

Most recently CNT+GNP nanocomposite with West Systems epoxy is analyzed under DMA showing a slight frequency dependence in the range of 1 Hz to 50 Hz. (Gbaguidi et al. 2017). T_g varies from 60℃ to 85℃ with increase in frequency and the frequency at which the loss of storage modulus occurs at 111 Hz.

4.3   DMA Characterization

Several studies have been done with SWNT/MWNT and epoxy/polymer composites, however very less work has been found for hybrid nanocomposites. It has also been observed that the storage modulus and glass transition temperatures of these composite depend greatly on the matrix properties and addition of SWNT/MWNT usually

have an increase in effect on these parameters. In order to investigate this affect DMA has been done of CNT+GNP/epoxy nanocomposites with 3M 2216 B/A translucent epoxy. DMA 8000 by Perkin Elmer is used without the nitrogen cooling and the equipment is shown in Figure 4.2.
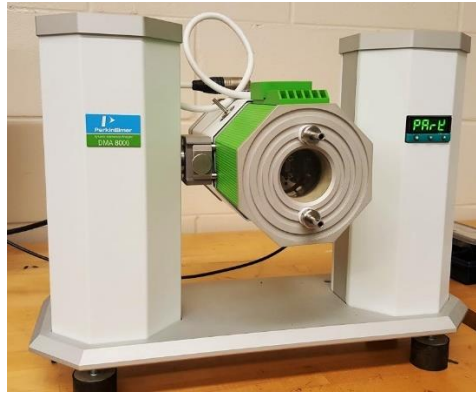
Figure 4.2 DMA 8000 by Perkin Elmer used for testing

Specimens of length 40 mm, width 6 mm, and thickness of about 0.2 mm are used for the DMA experiments, to examine the viscoelastic behavior of the nanocomposite. The sample are mounted in dual cantilever position in which the specimen is anchored on both ends by a fixed clamp and displacement is caused in the middle by the drive shaft as shown in the Figure 4.3 (a). Dual cantilever position is used for elastomers, thin films, and materials that have low stiffness. As the nanocomposite specimen lies under this category, therefore dual cantilever position is used for testing. The specimen mounted on the DMA is shown in Figure 4.3 (b).
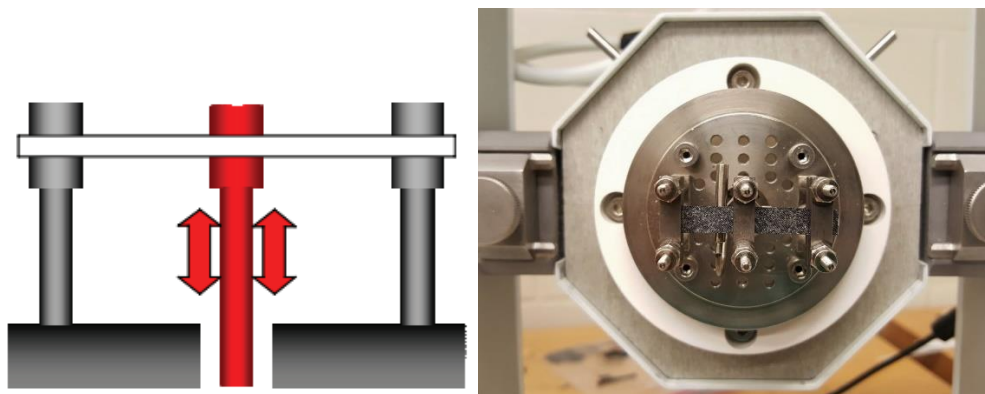
Figure 4.3 (a) Dual cantilever schematic (b) Specimen mounted on DMA 8000

4.3.1 Temperature Scan

Temperature scan is one of the most fundamental dynamic mechanical analysis test. The sample is heated at specific rate while the excitation is being applied and the variation in storage and loss moduli are observed. This gives an important parameter, i.e. glass transition temperature of the material. Glass transition temperature is specified by the temperature in which the elastic modulus decreases rapidly, usually by an order of magnitude or more. Often, for polymers, glass transition temperature is not a single value but a range of temperature.

For temperature scan, the specimen is first mounted in the dual cantilever bending clamps and a temperature scan of the nanocomposite is performed. Dimensions of the specimen are 40 mm × 6 mm × 0.2 mm. The specimen is heated from 30 °C to 100°C at the rate of 2 °C/min. Figure 4.4 shows the thermal scan of the nanocomposite for the frequency values of 1 Hz, 10 Hz, 30 Hz and 50 Hz. It can be observed that there is a drop in storage modulus from 30°C up to 60°C after which the curve flattens out. The storage modulus of the material starts decreasing as the temperature reaches near the glass transition temperature. However in this case, there is no flat region of curve in the

beginning. This suggests that the transition starts from the temperature below 30°C which could not be captured due to the limitation of the equipment. The overall response of the material is same for different frequencies in different temperature intervals, with slight frequency dependence. The value of storage modulus drops slightly as the frequency is increased, however slightly increased response at 30 Hz is observed. This is similar to the trend of CNT+GNP\West Systems epoxy composite, shown by Gbaguidi et al. (Gbaguidi et al. 2017).
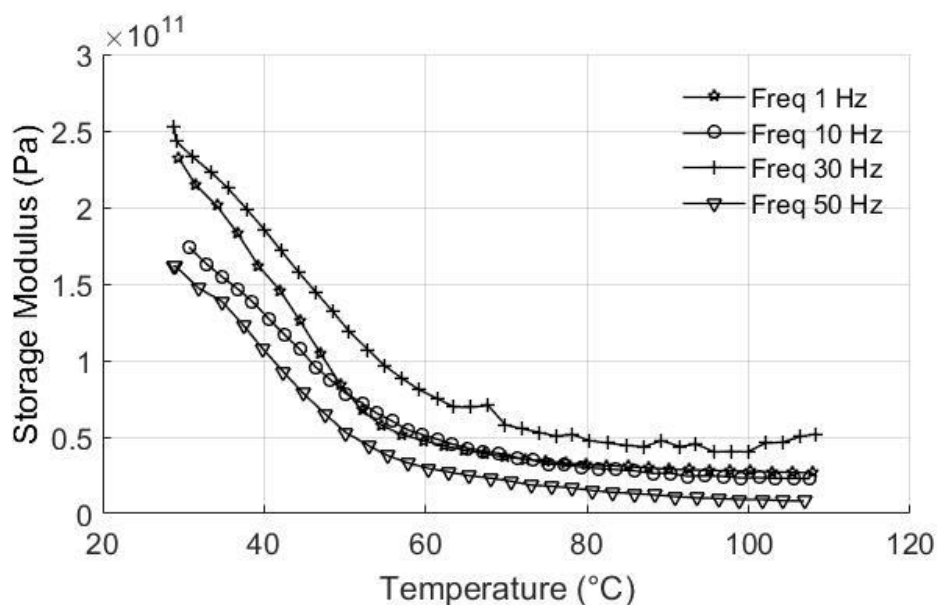
Figure 4.4 Variation in storage modulus with temperature at different frequencies

Figure 4.5 shows that the variation of tan delta with temperature. Tan delta shows a slightly broad peak around 50°C and 70°C depending on the frequency. Frequency dependence of the material leads to higher glass transition temperatures with higher frequencies. T_g values of 51°C, 64 °C, 75 °C respectively for frequencies of 1, 10 and 30 Hz. At 50 Hz, the maximum value of T_g occurs around 65°C followed by a broad peak. The glass transition values gives the thermal limit of effective use of these nanocomposites

for measure of deformations both in static and dynamic loading.
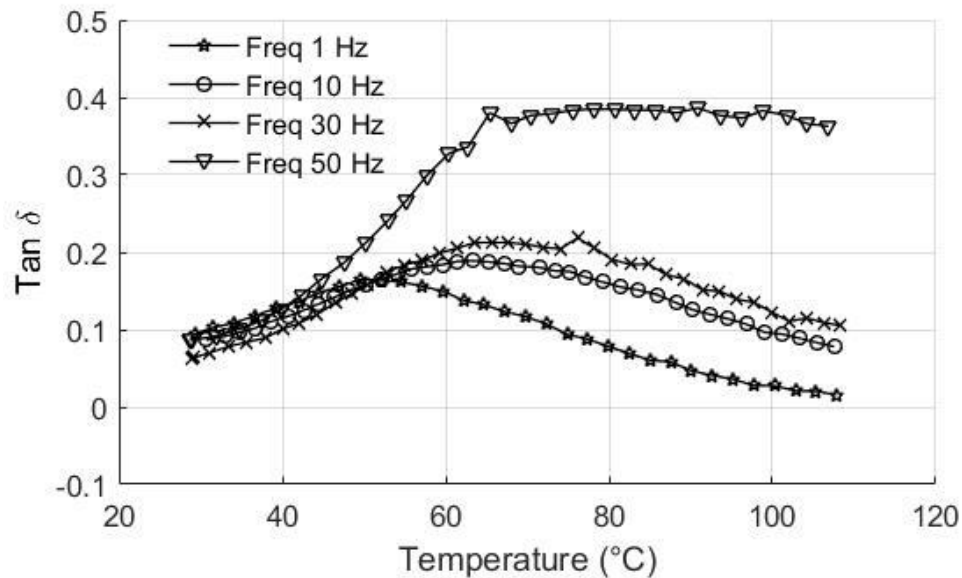
Figure 4.5 Variation of tan delta with temperature at various frequencies

4.3.2   Frequency Scan

Materials can go under various frequency loadings during their life. In this case, since it is an attempt to develop the piezoresistive nanocomposites as sensors, it is essential to know the material behavior with change in frequency. Excitation frequency can affect the modulus of the material in elastic phase, whereas in viscous phase, since the material flow phenomenon is dominant, frequency can have an effect on it.

In order to investigate this behavior, isothermal frequency scans of the nanocomposite is performed. The specimen, 40 mm × 6 mm × 0.2 mm in dimensions, is mounted in the dual cantilever position bending clamps an isothermal frequency scan is done at near room temperature. Figure 4.6 shows the variation of elastic modulus and tan delta with variation in frequency from 1 Hz to 200 Hz at 30°C. The values of modulus and tan delta are relatively similar in magnitude for low frequencies, i.e. from 1 Hz to 70 Hz.

However, after this a sudden drop of the modulus is observed at 81 Hz. This indicates that after this particular frequency, the modulus goes to zero, which indicates the total loss of material elastic properties and activation of viscous phase.
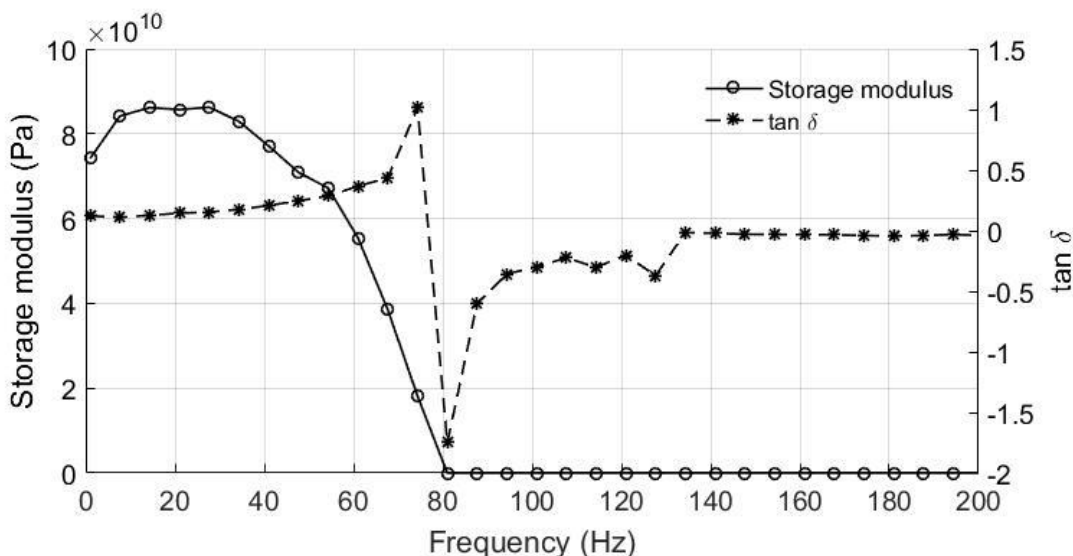
Figure 4.6 Storage modulus and Tan delta variation with frequency scan at 30°C

In order to observe the frequency response of the material w.r.t temperature, isothermal frequency scans have been at various temperatures, i.e. 30°C, 50°C, 70°C, 90°C and 110°C. The variation of storage modulus with frequency at these different temperatures is shown in Figure 4.7. It can be seen that with increase in temperature, the peaks shift towards bottom left of the graphs, which suggests that the storage modulus generally decreases with increase in temperature. It can be explained as, at higher temperatures, since the molecules are more energies in viscous phase, therefore they have less ability to store energy in form of work. The frequency at which total loss of storage modulus occurs, decreases at higher temperatures due to same reason.

Variation of tan delta with frequency at different temperatures is shown in Figure

4.8. Tan delta also has a similar trend as storage moduli. With increase in temperature, the curves shift towards left, i.e. the frequency at which storage modulus goes to zero decreases. This is the same trend as observed in Figure 4.7. Hence, frequency scan gives the frequency limit of the nanocomposite for its effective use in vibration testing at various temperatures. .
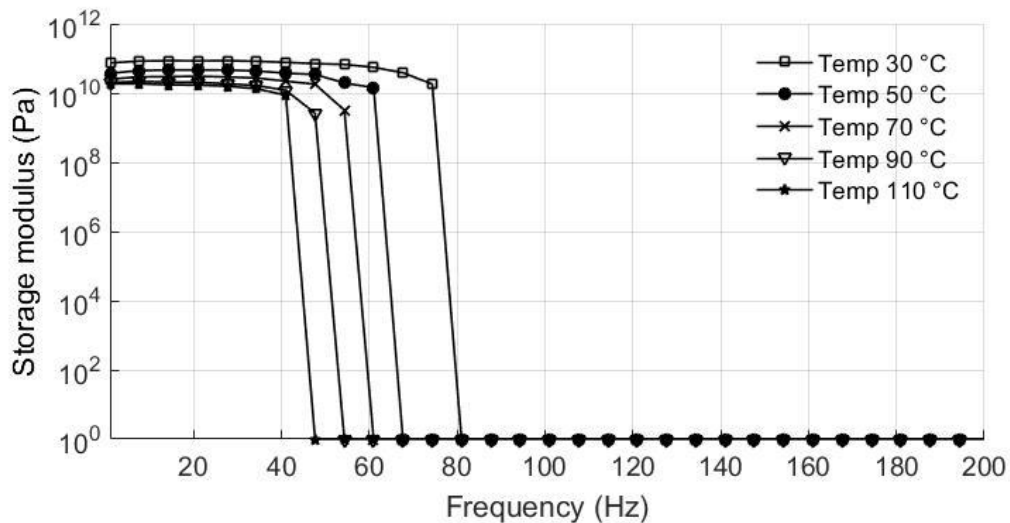
Figure 4.7 Comparison of storage moduli at different temperatures and frequencies
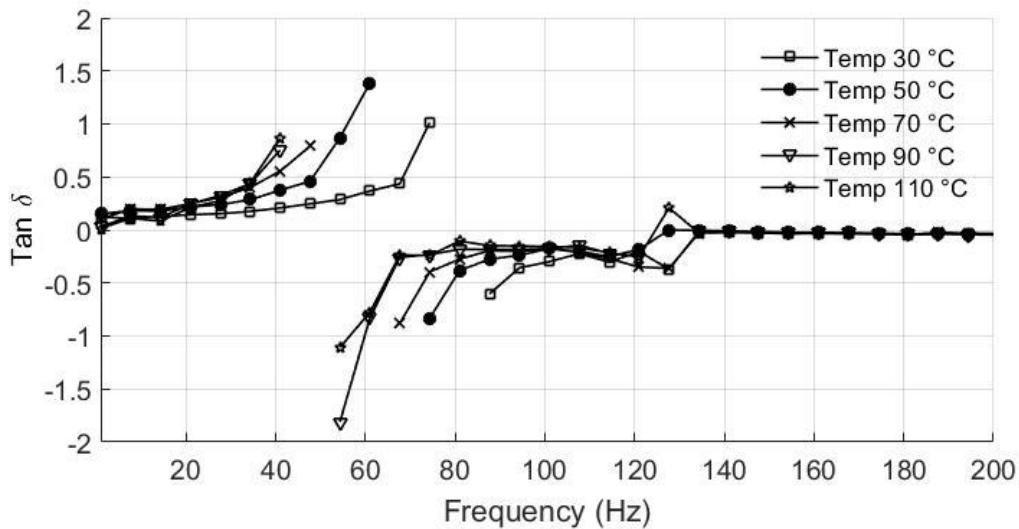
Figure 4.8 Comparison of tan delta at different temperatures and frequencies

The results suggest that the nanocomposite have both frequency and temperature dependence on its elastic properties. This effect is predominantly due to the epoxy matrix behavior and should be taken into account for use in static and dynamic sensing purposes.

5. Micrometeoroid and Orbital Debris Detection

5.1. Background

Inflatable structures for space habitat are highly prone to damage caused by micrometeoroid and orbital debris (MMOD) impacts. The size of orbital debris varies from few microns to meters but the probability of an impact increases significantly for particle diameter size of 0.001 cm to 1 cm due to their high flux. The velocity of these MMOD is very high, i.e. of the order of 1 km/s to 15 km/s with average velocity of about 9 km/s in lower earth's orbit (Christiansen 2009). Due to the high momentum, the material of the colliding particles has less significance, since even soft materials such as foams can cause damage and rupture of the structure. The disaster of the space shuttle Columbia is an example of such case where a piece of insulating foam struck the left wing of the orbiter. Depending on the size of the colliding particle, the induced damage may vary from micrometer size hole to rupture of whole structure.

Long term exposed space structures, such as International Space Station (ISS), face many such collisions throughout their service life, and therefore are shielded heavily against MMOD impacts. Even with safety precautions of shielding and orientation change, several incidents have been reported of damage to the ISS by MMOD, leading to the occurrence of a hole or a crack (Christiansen and Rollins 2012). If damage occurs to any of the pressurized structure such as habitat modules, it may result in a depressurization and leakage and can be a serious threat to the life of the astronauts. Therefore, it is very important to know of any event of impact occurrences as well as severity of damage as early as possible.

Existing space structures have been using different sensors for impact detection.

After the loss of Columbia, the Space Shuttle Orbiter was equipped with wing leading edge impact detection system (WLEIDS) to qualitatively estimate the impact and location of damage for a limited period of time (Studor and George 2007).

Currently the techniques used by NASA and other space agencies to detect the damage occurrences vary from pressure sensors for leak detection, monitoring cameras to inspect the damage through images, ultrasonic testing to other NDE techniques (Koshti 2015). There is a great need for a structural health monitoring system that can detect impact damage, such as its location and severity, and keep the crew updated with the health of the structure.

5.2. Literature Review

There are several different approaches for damage detection caused due to MMOD impact that have been reported in literature. One method is to develop a blanket/layer that covers the whole structure and MMOD impact is found by the damage in blanket layer. A second approach can be the installation of sensors on the existing structure that can remotely detect the event of impact. Similar attempts have been made in the past; Brandon et al. developed a blanket type layer with wireless communication, which works on the principle of a capacitor (Brandon et. al., 2011). When a capacitor is damaged due to the hole created by the impact, capacitance of the sensor changes due to change in the area, and this can be used to get information about the event of impact. The layer consists of number of such sensors installed in array to cover the whole structure. Similarly, Woodard et al. used open-circuit electrically conductive spiral trace sensor for damage detection (Woodard et al. 2011). Due to damage, the magnetic field response of the sensor changes that can be used for detection. Moreover, piezoelectric film sensor layer (Christiansen

2009) and conductive traces (Lewis and Island 2016) were used as a coating material or embedded between the laminates for sensing purposes. Fiber optics were also woven inside a fabric to provide an indication of damage through strain sensing (Cadogan et al. 2006).

Imaging by scanning the habitat walls with different electromagnetic radiation wavelengths has also been studied for MMOD damage detection and yielded positive results (Madaras et al. 2008). More complex techniques involved the use of acoustic and impedance tomography to provide information about the location of damage in the layer. Current and future research towards space habitat structures is directed towards inflatable structures for easier transportation and much less volume and weight. This consists of multiple layers of different materials which are flexible and can be deployed once in the structure is in space. The typical inflatable space structure and its shell layer configuration are shown in the Figure 5.1.
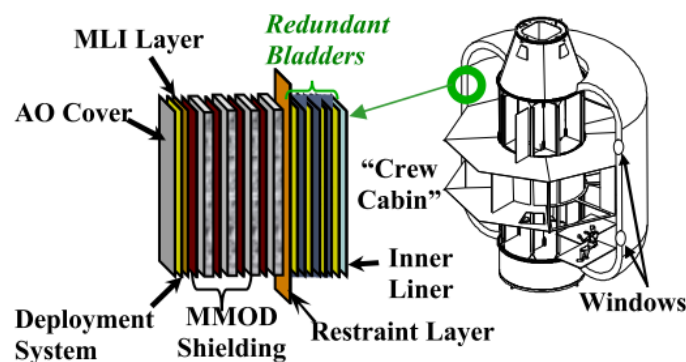
Figure 5.1 Typical configuration of inflatable structure and shell layers (Fuente et al. 2000)

The requirements for an integrated structural health monitoring system for inflatable are that it should provide the information of occurrence and time of impact, location of damage, depth of penetration, and the extent of the resulting damage. According to Valle (Es and Valle 2012), the inflatable structural health inspection systems should

monitor prelaunch packaged state, on-orbit functionality before deployment, initial deployment validation, and on-orbit operation using embedded sensors. Sensing equipment would need to tolerate packing and folding without creating sharp edges that can damage the fabric and films. They should undergo stowage and be able to resist mechanical pressure during deployment. It would also need to tolerate flight conditions and ground handling.

5.3. Approach

In this study, the potential of CNT+GNP/epoxy nanocomposites to detect the damage caused due to MMOD impact and potential of use for SHM system for inflatable structures is investigated. Thin flexible layer of these nanocomposite when incorporated between soft good layers of the inflatable structure can act as sensing layer. An array of these sensors can be used to develop a sensing layer, which when sandwiched between soft good layers in a space habitat can provide MMOD detection capability. A schematic of such a layer in inflatable structure and sensing array is shown in Figure 5.2.
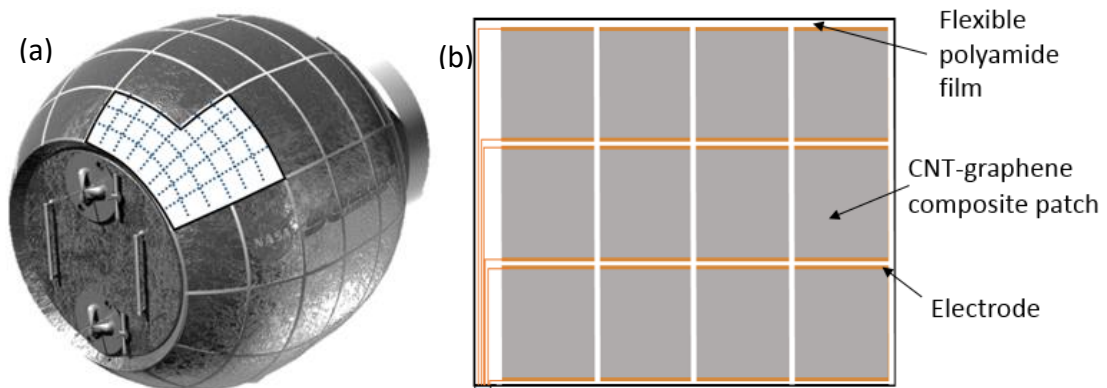
Figure 5.2 (a) Schematic depiction of sensor array configuration and (b) tile and grid sensing patterns (Figures from NASA STTR project meetings with LUNA, 2017)

In an event of impact, a hole could be created in the sensor, which would change the resistance of that particular sensor. This change is measured and fed to the computer algorithm that determines the severity of damage by measuring the amount of change in electrical conductivity. The entire layer is scanned after a preset amount of time, which provides the interval of impact occurrences. The damaged sensor's identification can provide information about location of the damage. The sensing layer is sandwiched between Kapton layers for protection and insulation. These sensing layers can be stacked among the material layers at multiple locations, which can provide the information about depth perception of the damage.

An MMOD event will cause a hole/rupture in the inflatable and sensing layer. Detecting the hole caused due to MMOD impact can provide information about the damage caused due to it. In subsequent sections, the response of nanocomposite will be studied as the holes are created in the nanocomposite sensors. The effect of different epoxy matrices and addition of coarse graphene platelets will be discussed. Effect on size of specimen and damage detection in case of multiple specimen will be studied. Damage detection for multiple layers will be briefly discussed as well. Table 5.1 provides information about the impact studies and hole characteristics that have been done previously.

Table 5.1 Size of hole created due to MMOD based on projectile size (Christiansen 2009)

Spherical Projectile diameter (∅)	Velocity	Hole Size	Target Material	Depth of penetration
3.7 mm	11 km/s		Double aluminum bumper	Through
0.8 mm	7.1 km/s	3 mm 5 mm	Reinforced Carbon-Carbon	Through
1.27 cm	5.8 km/s	1.6 cm	Stuffed Whipple and	Through

Spherical Projectile diameter (∅)	Velocity	Hole Size	all-Aluminum Shield	
			Target Material	Depth of penetration
0.8 mm	5 km/s	3 mm	Aluminum	Through
0.3 mm	5 km/s		Aluminum	Partial
1 mm		1 mm	Kapton	Through
1 mm	6.9 km/s	4.1 mm	Copper polyamide film based sensor	Thru
2.7	7.27 km/s	6 mm		
0.32 cm	6.59 km/s	2 cm by 3 cm, 3.8 max dia.	PICA	Through

It can be seen that the impact causes a through hole in most of the cases irrespective of the target material. This is obviously due to very high velocity of the impact projectile. The size of hole caused varies with the size and velocity of the projectile and the target material and its location in case of sandwiched structure. 3 mm hole size is taken as reference as standard minimum damage size to study the response of piezoresistive nanocomposite.

5.4.   Single sensor performance

Firstly, the electrical response of the single sensor to addition of 3 mm hole is inspected. Effect of sensor size, matrix material and number of holes on single specimen are investigated.

5.4.1. Electrical resistance of 2.5 in × 0.5 in nanocomposites

In this section, the results of electrical resistance measurements of the 2.5 in × 0.5 in nanocomposites with addition of holes are presented. Four different type of specimen are made (a) neat bucky paper and west systems epoxy, (b) neat bucky paper and 3M 2216 translucent epoxy, (c) coarse graphene platelets (5 wt. %) and neat bucky paper with west

systems epoxy, (d) coarse graphene platelets and neat bucky paper with 3M 2216 translucent epoxy. All specimen are made with the dimensions 2.5 in × 0.5 in. and tested with a current value of 0.05A using four point probe measurement method. Four successive holes of approximately 3 mm diameter are added in each specimen. Figure 5.3 shows all four types of specimen with added holes. The specimen were coated with Kapton tape for protection as to be expected in the actual sensing layer.
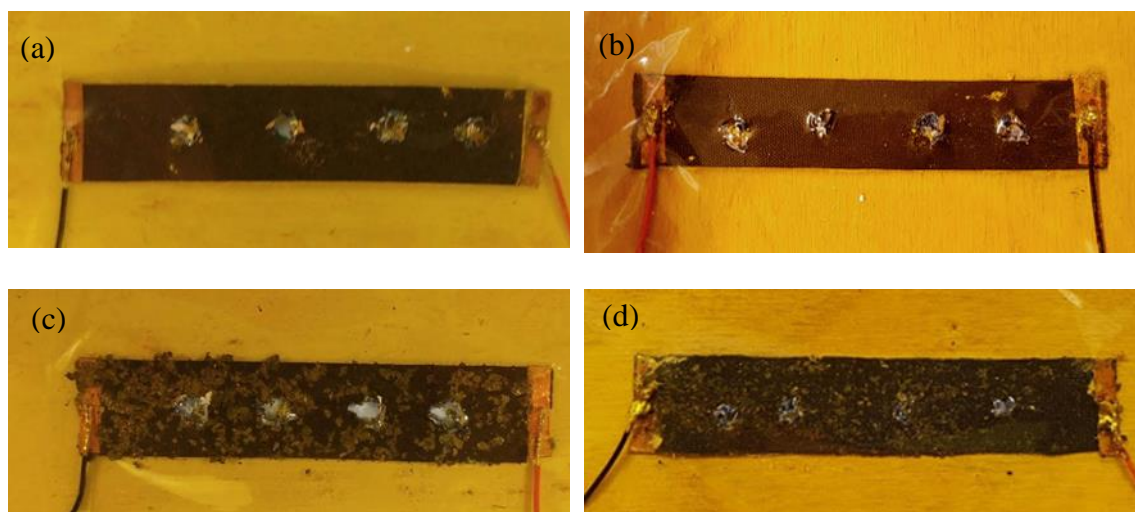
Figure 5.3 Different types of $2.5\ in \times 0.5\ in$ nanocomposites covered with Kapton tape and 4 holes added. (a) CNT/West Systems epoxy (b) CNT/2216 Translucent epoxy, (c) CNT+GNP/West Systems epoxy and (d) CNT+GNP/2216 translucent epoxy composites

A period of 1 min to 5 min is observed before addition of any hole, in order to see if there is any changes in resistance values, but it is found to be steady. Figure 5.4 shows change in resistance with addition of holes in case of neat bucky paper with 3M 2216 translucent epoxy. We can see a clear and noticeable increase of the electrical resistance, by at least 5%, every time a hole is added to the neat bucky paper with 3M 2216 translucent epoxy nanocomposite. In addition, we observe that the resistance of the specimen remains constant after any addition of hole, which proves the stability of the specimen in detecting holes.
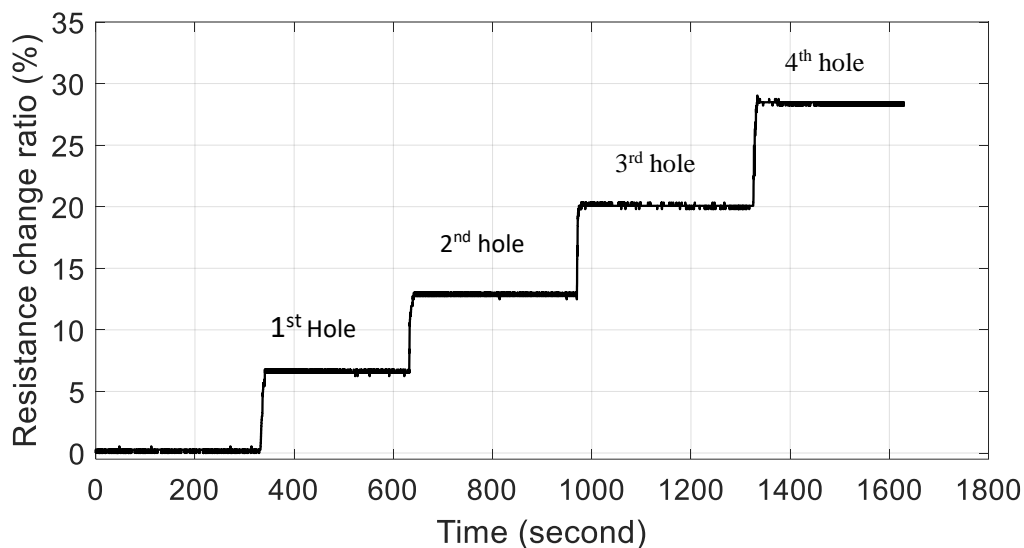
Figure 5.4: Variation of resistance change ratio with time and addition of size of holes to a 2.5 in × 0.5 in. coarse graphene platelets based nanocomposite.

Figure 5.5 shows the comparison of resistance change ratio with addition of holes for different types of composite, i.e. a) Neat bucky paper with West Systems epoxy, b) Neat bucky paper with 3M 2216 translucent epoxy, c) neat bucky paper with coarse graphene platelets and west systems epoxy, d) neat bucky paper with coarse graphene platelets and 3M 2216 Translucent epoxy. As seen from the plot, the behavior of both epoxy matrices is same on the resistance change with addition of holes. 2.5% increase in resistance change ratio is observed for neat bucky paper. However when coarse graphene platelets are added, the change increases significantly to almost double the value, i.e. 5%. This tends to show that epoxy matrix does not have much effect on the sensor performance, however, the addition of coarse graphene platelets significantly increases the sensitivity of the nanocomposites to holes.
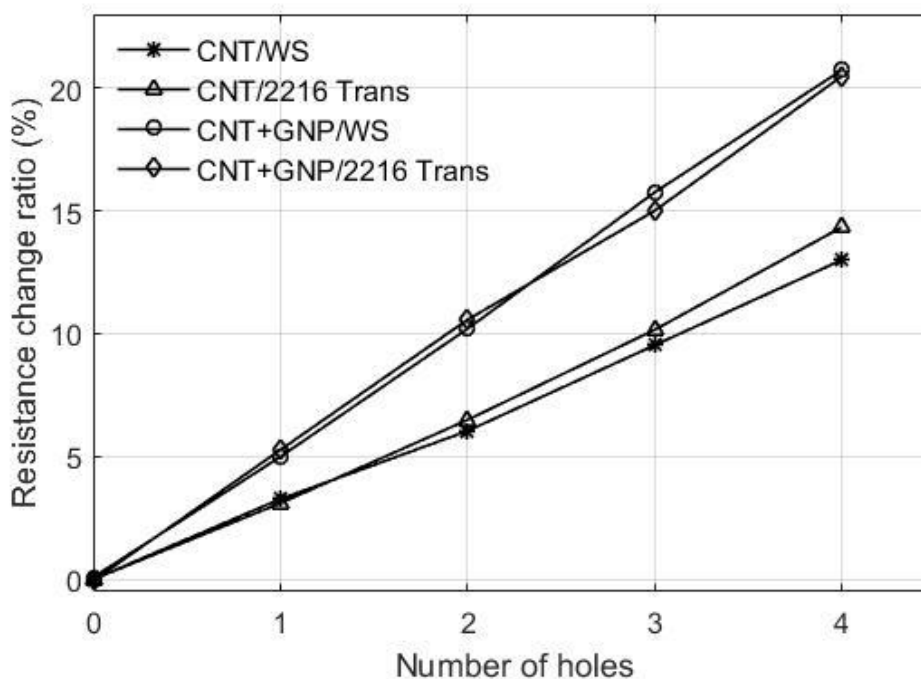
Figure 5.5 Variation of resistance change ratio with addition of holes to 2.5 in×0.5 in. CNT/West Systems epoxy, CNT/2216 Translucent epoxy, CNT+GNP/West Systems epoxy and CNT+GNP/2216 translucent epoxy nanocomposites.

5.4.2. Electrical resistance of 2.5 in × 2.5 in nanocomposites

According to the previous results, addition of coarse graphene platelets to the nanocomposites gives the highest sensitivity to drilled holes compared to neat buckypaper-epoxy nanocomposites. In order to cover a larger area by each sensor on sensing layer, the sensor size should be large enough otherwise it will increase the number of sensors in each layer a lot and also will complicate the system. To address this issue, sensors are developed with dimensions 2.5 in × 2.5 in. one large sensor will be equivalent to 5 smaller sensors of 2.5 in × 0.5 in. size. 2.5 in × 0.25 in copper electrodes and wires are attached at both ends to measure the resistance, while 0.5A current is passed through it. (See Figure 5.6)
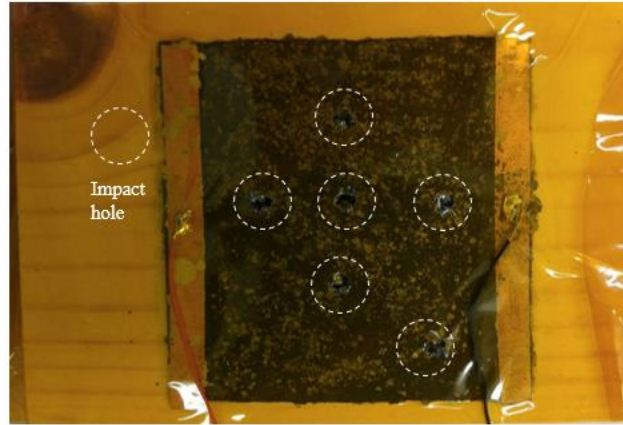
Figure 5.6 2.5 $in \times$ 2.5 in nanocomposites covered with Kapton tape. Six Φ3mm holes are successively added.

This larger nanocomposite specimen also exhibits change in resistance when holes are added. Figure 5.7 shows the resistance change ratio of one of the composites with time and with addition of holes in the specimen. As explained before, a period of 3 min to 4 min is observed before addition of any hole. A clear and noticeable increase of the electrical resistance can be observed, by at least 0.75%, every time a hole is added to the material. Also the resistance of the specimen remains constant after any addition of hole, which proves the stability of the specimen in detecting holes. Figure 5.8 shows the variation of the resistance change ratio with addition of holes. The data used correspond to an average of several samples. It can be noticed that the resistance change with the 2.5 $in \times$ 2.5 in specimen is lower than the one obtained with the 2.5 $in \times$ 0.5 in specimen. This is due to the fact that the length-to-width ratio of the specimen has been decreased which decreases the resistance of the specimen itself.
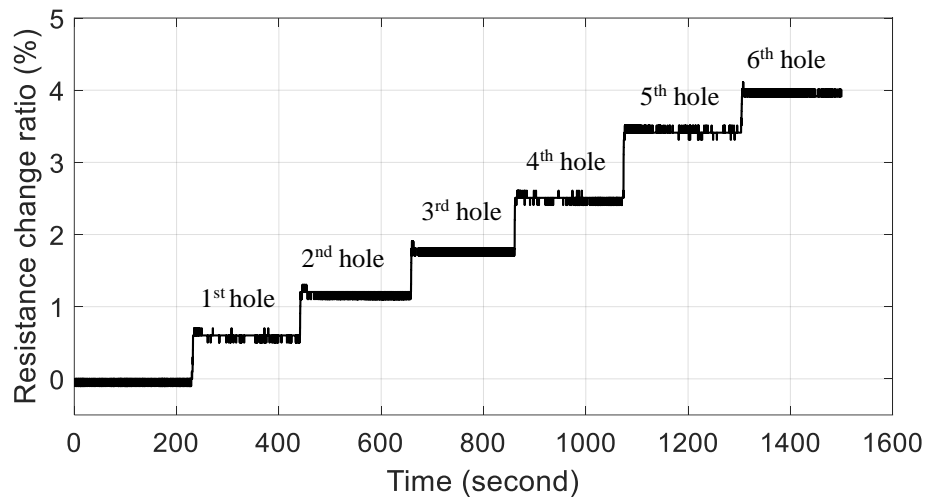
Figure 5.7. Variation of resistance change with time by addition of holes to a 2.5 in x 2.5 in coarse graphene platelets based nanocomposite sensor
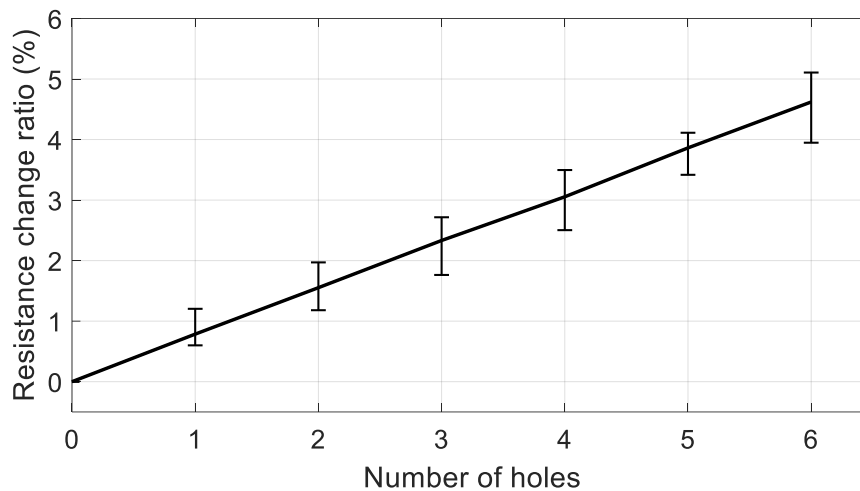
Figure 5.8. Averaged variation of resistance change with addition of holes for several $2.5\ in \times 2.5\ in$ coarse graphene platelets based nanocomposites.

Finally, to test the performance of this new specimen with a large number of holes, 20 holes are introduced to the specimen to see if the sensitivity of the specimen remains consistent. (See Figure 5.9). Figure 5.10 shows that the specimen remains equally stable and sensitive even with a much larger number of holes.

Figure 5.9. 2.5 in × 2.5 in nanocomposites made of covered with Kapton and twenty Φ3mm holes are successively added.
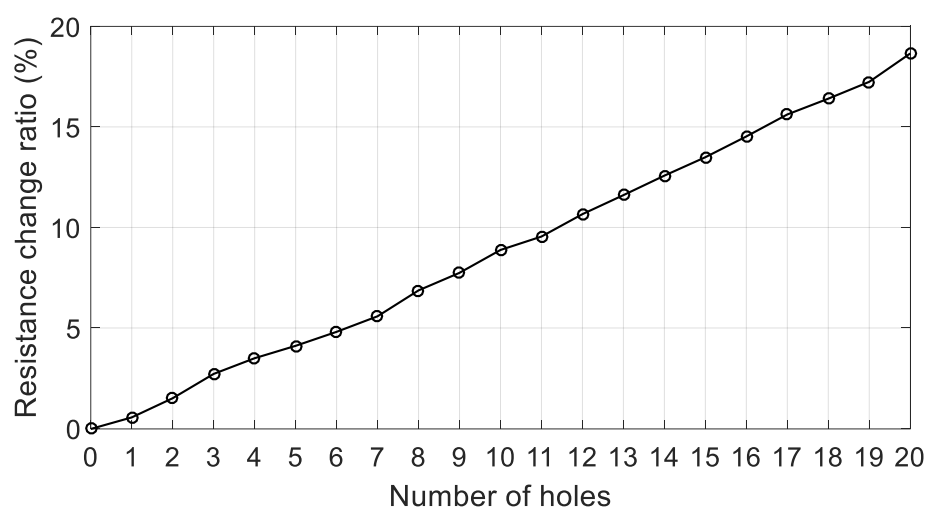
Figure 5.10 Variation of resistance change ratio with addition of 20 holes to a 2.5 in × 2.5 in coarse graphene platelets based nanocomposite.

5.5.   Multiple sensor configuration

5.5.1. Sensor array testing

In order to demonstrate how the multiple sensors will form an array to cover larger area, four sensors are placed together to form a 2×2 array (see Figure 5.13 (a)). Although each sensor requires a very small amount of power, for a large array, the power requirement would be multiplied by the number of sensors used. To develop a power efficient system to meet the demanding power budget in space applications, an electronic control circuit is developed to periodically pass the required amount of current through a particular sensor

in an array of four sensors. The control circuit consists of a current supply and a switching mechanism that distributes the desired current, i.e. 0.5 amperes at 12 volts, through each sensor for a preset time interval. Additionally, it can monitor the four sensors simultaneously or separately. The sensors can be scanned in a periodic or a continuous scanning mode. The circuit design and the developed circuit are shown in Fig. 5.11 (a) and Fig. 5.11 (b), respectively. This concept can be easily expanded when dealing with more sensors.
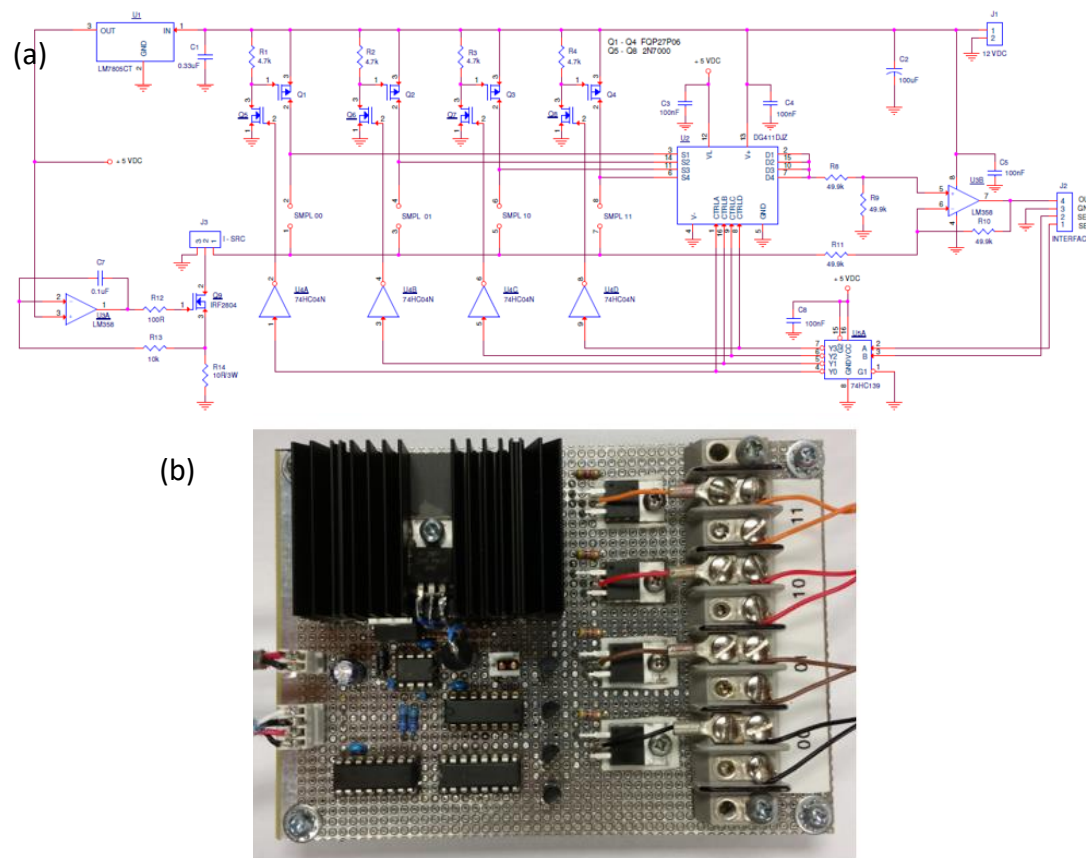
Figure 5.11. (a) Circuit schematic for periodic sensor scanning and (b) circuit for impact monitoring panel.

A LabVIEW Visual Interface (VI) was developed to facilitate this process. The software stores the data obtained through each sensor and calculates the damage indices to detect the impact holes. Moreover, the VI displays the damage indication and updates the

sensor data each time the scan is performed. If the change in resistance is more than a preset threshold, damage is indicated by turning LED light to different color in the front control panel. This approach can be used for multiple sensors on a panel or on sensors at different depths. The circuit and the control panel were used to test a multilayer damage detection event using a low velocity impact test.

Figure 5.12(a) shows a four sensor array in which the top right sensor is damaged by drilling a 3 mm hole. Figure 4.12(b) shows the LABVIEW VI which displays the resistance changes in each of the sensor from the previous state. It can be seen that with the hole in sensor 1 (top left sensor) change in resistance is observed from the graph. Meanwhile LED turns red as an indication of damage in the respective sensor.
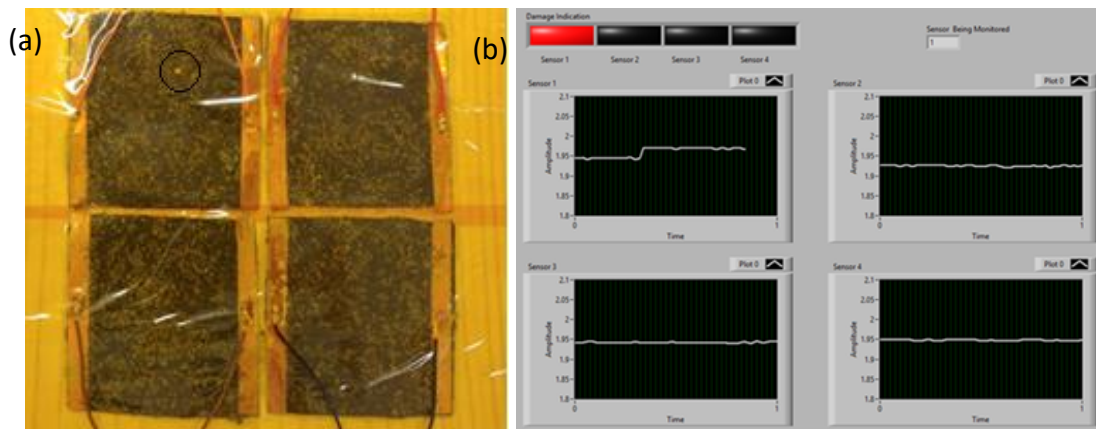
Figure 5.12. (a) Four sensor array with a hole in top left sensor and (b) LABVIEW VI displaying change in resistance and indication of damage in respective sensor.

5.5.2. Multi-layer impact testing

As discussed earlier, the inflatable structure consists of multiple layers sandwiched together for protection against the environment. In the event of an impact, as the particle collides with the first/outermost layer, it starts shattering into pieces. As it continues to impenetrate through the subsequent layers, the momentum of the particle exponentially

reduces. On the other hand, the colliding particles shatters in to smaller and smaller pieces and forms a tiny cloud of particles which increase the damage area on the subsequent inflatable layers. This damage extent comparison of front and rear layers is shown in shown in Figure 5.13.

(a)   (b)
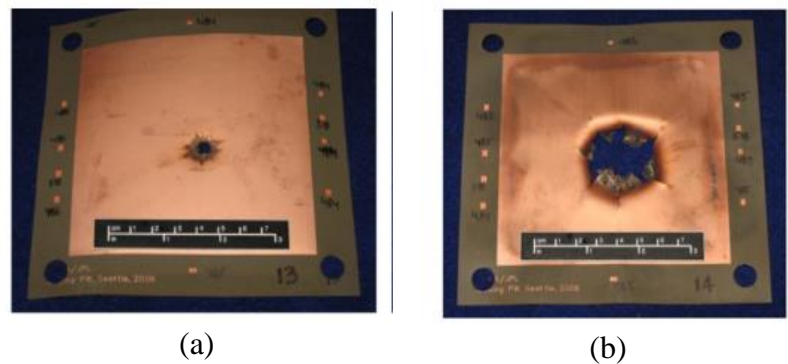
Figure 5.13 Comparision of damage on (a) impact facing versus (b) rear layer (Brandon et al. 2011)

For multi-layer testing, impact testing has been done (Anees, et al., 2017) in which the same idea has been employed. The nanocomposite sensor was bonded to a dry fiberglass substrate, which represents the soft goods layer of an inflatable. Two fiberglass layers four inches apart at the top and bottom are placed in a specially designed test fixture and subjected to low velocity impact test in Instron Dynatup 9250 drop tower. Variable thickness indenter has been used to create 6 mm and 3 mm diameter holes in the upper and lower layers respectively. The test fixture, indenter, and test setup are shown in Fig. 4.13.

During the impact, as the indenter will pass through the layers, top layer will be impacted by the 3 mm diameter segment first, followed by the 6 mm diameter segment, eventually creating a hole of at least 6 mm. The bottom layer however will be subjected to 3 mm diameter segment only and hence will have a hole of 3 mm approximately. This is reverse case of the actual scenario in inflatable structure, where the outermost layers have

much smaller damage and the damage size will increase at each successive layer. However since the sensors in different layers will be just having different damaged areas, so in essence the test represents a similar scenario of actual case, where if the different damage sizes can be detected, it can be stated that different layers can also be distinguished.
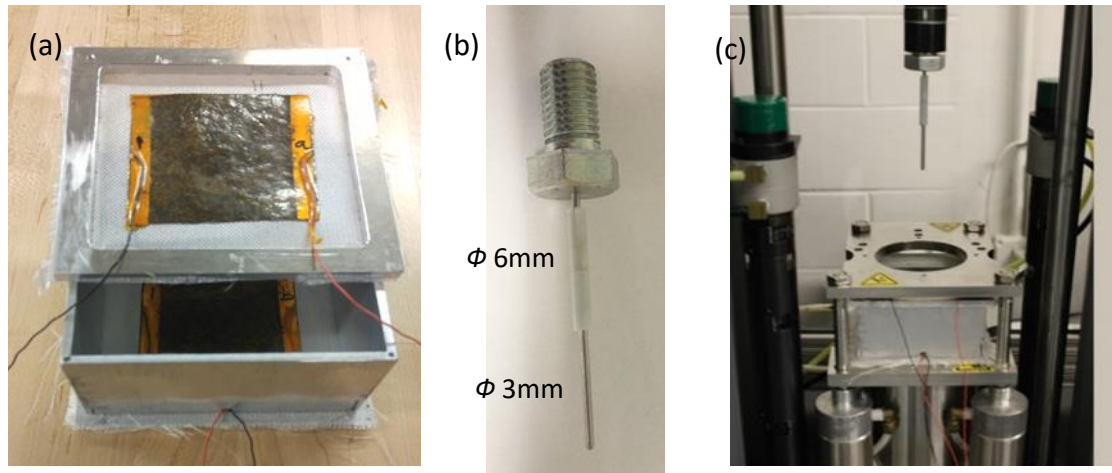
Figure 5.14. Double layer Impact setup: (a) two sensors mounted on the fixture, (b) indenter with different thickness along its length, and (c) test setup in the machine.

A LabVIEW program has been made to distinguish between different damage sizes based on the difference in change in resistance. Figure 5.15 shows the LabVIEW front panel that indicates impact damages caused on top and bottom layers. The red indication on the left hand side shows that the damage has been done to both the layers, i.e. top and bottom layer, since the indenter has hit both the layers. The yellow indicator on the right hand side indicates that only the top layer has the large damage whereas the bottom layer does not shows any large damage, as only the top layer has been struck by the 6 mm segment of the indenter. The results show the capability of sensor system and the program to monitor detect damage among different layers and differentiate between large and small damages based on the preset value in the program.
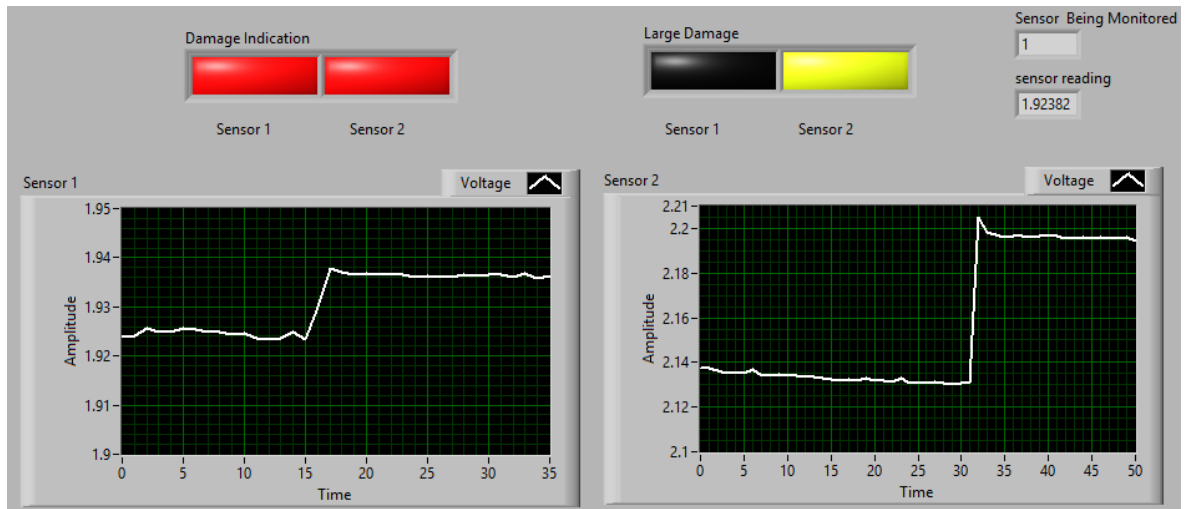
Figure 5.15 LabVIEW VI displaying damage indication on top and bottom layer, versus large damage only on top layer

This shows that GNP-CNT epoxy based piezoresistive nanocomposites can be used for damage detection caused due to MMOD impact between layers of inflatable structure and can provide location and extent of damage among different layers.

6. Outgassing testing

The materials exposed to space environment are subjected to extreme space conditions. These include high vacuum, electromagnetic radiations, and high temperatures variation along the life of the structure. These environmental conditions have variation depending on the type of mission type, and material application. NASA requires all the spacecraft materials to be space qualified and one of the important parameter is outgassing testing. Outgassing is the amount of gas released in vacuum that was stored, trapped or absorbed by the material during its processing in atmospheric environment. Outgassing mostly occurs when the materials are exposed to heat under vacuum conditions. Usually polymers and epoxies have high outgassing properties and therefore are more prone to risk, therefore they are required to pass the outgassing requirements.

There are three most common parameters to describe the outgassing properties, i.e. Total Mass Loss (TML), Collected Volatile Condensable material (CVCM) and Water Vapor Regained (WVR). TML is the total mass lost from the material when the material is kept at constant temperature and pressure for a specified period of time. TML is calculated by the formula

$$TML = \frac{W_0 - W_f}{W_0} \times 100$$

Where W_0 is the initial weight of the specimen before the outgassing test and W_f is the final weight of the specimen after the test. CVCM is the quantity that has been outgassed from the material and collected after condensation at particular temperature and pressure. CVCM is calculated from the percentage difference in condensed mass on the collector before and after the test. WVR is the amount of water regained by the specimen when the specimen is conditioned to atmospheric pressure at specific temperature and

humidity after the test. WVR is calculated from the percentage difference in weights of specimen before and after the conditioning. The outgassing requirements from NASA in order for the material to qualify for space use are TML < 1.0 % and CVCM < 0.1% when the testing has been done in accordance with ASTM E595-15 standard.

ASTM E595-15 standard, explains about the testing conditions, the critical parts of the apparatus that needs to be met in order to get reliable, and reportable outgassing data. The schematic of the apparatus is shown in the Figure 6.1. The material is placed in the material chamber and the he test conditions required are given in Table 6.1. The material is prepared according to the standard procedure, weighed and then placed in the specimen compartment and heated at the specific temperature. The pressure of the test chamber is maintained at the required value and the material is exposed to these conditions for 24 hrs. Due to vacuum, some amount of material is lost which is collected at the collector plate. TML and CVCM values are then calculated to determine the amount of material loss by weighing the specimen.
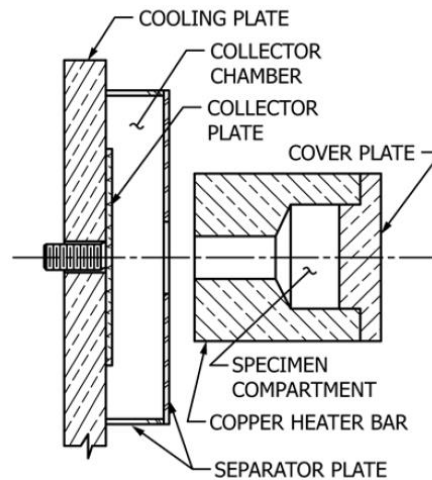
Figure 6.1 Schematic of critical portion of the apparatus (ASTM 2015)

Table 6.1 ASTM outgas testing parameters

Parameter	Required value
Material weight	200-300 mg
Material heating temperature	125°C or 30°C more than maximum service temperature
Vacuum pressure	$<10^{-5}$ torr
Time duration	24 hrs.
Collector plate temperature	25°C

6.1. Literature Review

There is significant amount of data available online regarding outgassing properties of various polymers and epoxies by NASA (Powers n.d.). However this data is mostly for commonly and commercially available materials. For a composite material, constituent material data cannot be taken as reference and the composite material needs to be tested separately. For CNT/epoxy based nanocomposites, very limited researchers have reported outgassing values. Outgassing has been done with non-standard procedures for various epoxy composites during the preparation, in order to evaporate the solvent. For example, Jung et al. (Jing Li, Wong, and Kim 2008) outgassed the Epon 828 epoxy at 80 °C for 2 hr. during the fabrication of the CNT+GNP/epoxy hybrid nanocomposite. Shan et al. (Sham and Kim 2006) performed outgassing of MWNT/Epon 828 epox composite at 80 °C overnight for nanocomposite fabrication. Similarly outgassing of acetone is done for 1 h at 100 °C in preparation of poly(2-hydroxyethyl methacrylate) (PHEMA)/MWNT composites (Xu et al. 2010). Polytetrafluoroethylene (PTFE)/SWNT nanocomposites (Vail et al. 2009) and CNT/PEEK (McCook et al. 2007) based nanocomposites have been prepared due to low-outgassing of PTFE and PEEK for use in space applications, however not any results of low outgassing of the final product were shown. All of these outgassing tests have been conducted in non-standard way only for composite development.

Only outgassing testing of epoxy resin (PRIME LV 20, Gurit) reinforced with commercial MWCNT powder at 0.5, 2 and 2.5 wt% have been according to ASTM standard (Micheli et al. 2012). Test results reveal that TML value of 1.23% was observed which is slightly higher than the required value of <1.0%. However CVCM, WVR and Recovered Mass Loos (RML=TML-WVR) values were found to be satisfactory.

The TML value of 3M 2216 B/A gray epoxy has been given to be 0.77% (3M 2009) which is desirable but 2216 B/A gray epoxy is not used for nanocomposite development. It is because of the high viscosity, the epoxy tears the layers of the buckypaper during fabrication of the nanocomposite. This is shown in Figure 6.2

Figure 6.2 Tearing of layers of buckypaper due to application of 3M 2216 B/A gray epoxy

The TML value of 3M 2216 B/A translucent epoxy is not available in the literature. It is expected that the TML value of translucent epoxy could be somewhat closer to the 3M 2216 B/A gray epoxy because of its similar nature, however it cannot be said with surety. Moreover since the TML of the composite will differ from the TML of matrix alone, therefore it is essential to investigate the TML of the nanocomposites.

6.2. Approach

The MMOD detection layer is to be placed between the layers of the walls of the inflatable structure. The hot temperatures will be experienced during the launch phase, closer to earth whereas during deep space mission, inflatable structure will be exposed to cold phase during most of its mission. Since the layer is covered form thermal isolative layers from outside, therefore the temperature range experienced by the MMOD detection layer is given to be between -45°C and +10°C (+/- 50°F). Since the maximum outgassing occurs at the highest temperature, therefore the maximum material testing temperature is 40°C.

Apparatus has been designed to perform outgassing testing according to ASTM standard. It consists of 9 specimen compartments, out of which 3 compartments can act as control to quantify any cross contamination and 2 types of samples, each in 3 quantity can be tested simultaneously. The heating is done using heater rods attached to the heating plate, while Peltier devices are used to keep the cooling plate at 25°C. Most of the critical dimensions of the apparatus mentioned in the ASTM standard have been met, except very few that required very fine thickness or tolerances, i.e. in order of micrometers due to limitation of available resources. However the modifications are made in a way to maintain the design integrity as best as possible and it is expected that these modifications would not have any significant effect on the TML values. CAD model of the apparatus in CATIA is shown in Figure 6.3.
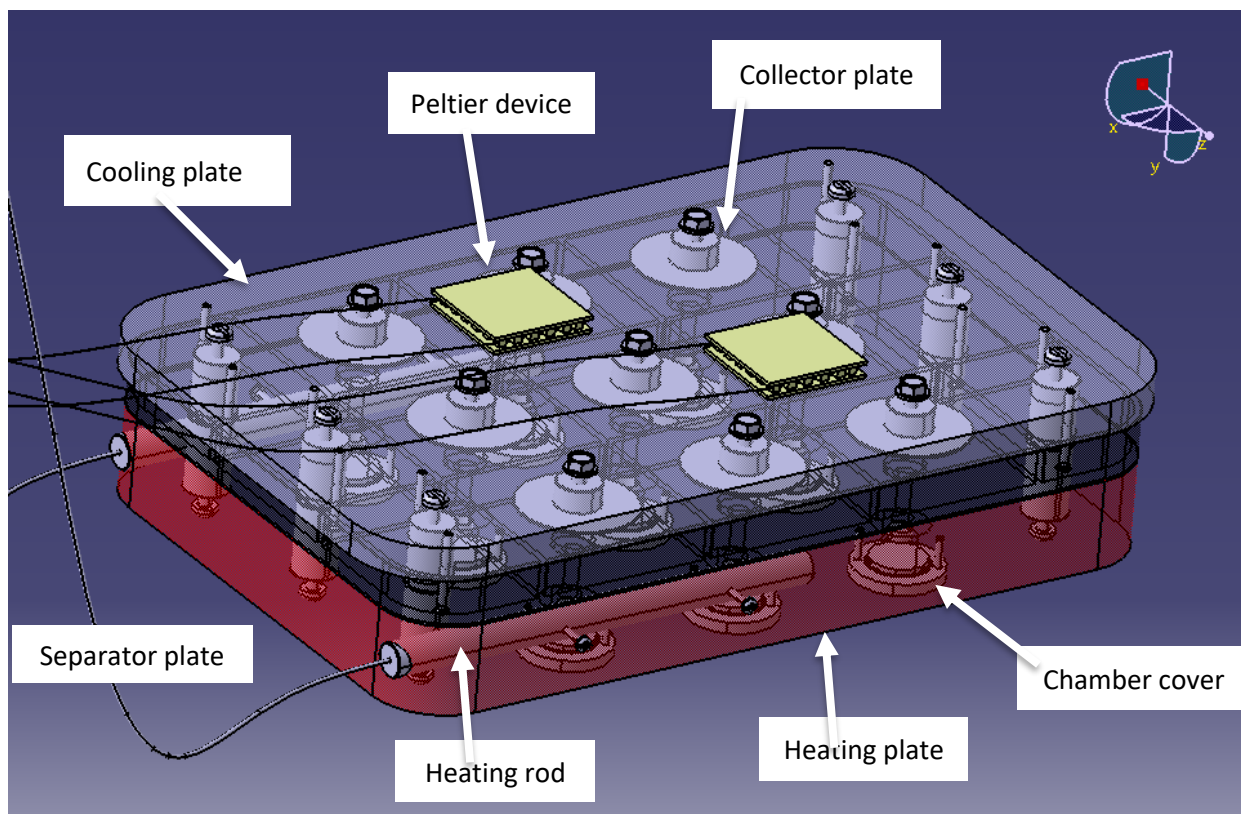
Figure 6.3 CAD Model of the apparatus designed for outgassing testing

6.3. Test procedure

An in-house developed vacuum chamber (shown in Figure 6.4) has been used for the outgassing testing, Due to the unviability of the designed apparatus and limitation of the vacuum chamber, the test specimen are exposed to pressure of 5×10^{-3} torr for 24 hours at room temperature to calculate the TML values.

In order to get a clear picture of behavior of different constituent materials in the nanocomposite, three different types of samples are prepared. These are

1) CNT buckypaper cured with 3M 2216 translucent epoxy

2) CNT buckypaper and coarse graphene platelets (GNP) composite cured with 3M 2216 translucent epoxy (CNT+GP/2216 Trans)

3) CNT+GP/2216 Translucent epoxy nanocomposite coated with Kapton tape on both sides.
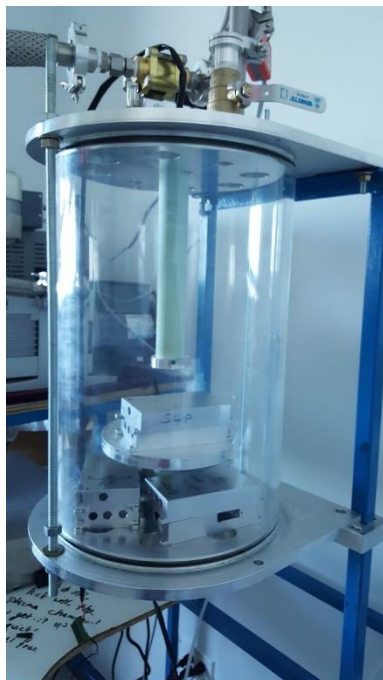
Figure 6.4 Vacuum chamber for outgasssing testing

Composite samples were prepared with the standard method of preparation. Specimen were handled with clean nylon gloves and stored in plastic bags to avoid any contamination. The specimen were weighed between 200 mg to 300 mg and cut into appropriate sizes. Before the test, specimen were conditioned at 23 ℃ for 24 hours in the environment chamber. Specimen were weighed with a scale of 0.1 mg accuracy, just before placing them in the aluminum housings and the vacuum chamber. Due to unavailability of the designed apparatus, aluminum housings covered with lids, also called as boats, were used to act as specimen containers for the test. The boats were cleaned thoroughly using 99.952% isopropyl alcohol before the test. Figure 6.5 shows all three types of specimen placed in the housings.
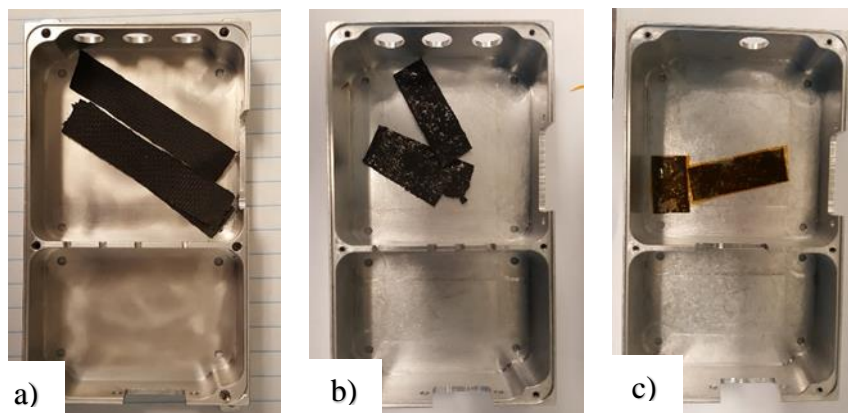
Figure 6.5 (a) CNT/2216 Trans epoxy (b) CNT+GP/2216 Trans epoxy, (c) CNT+GP/Trans epoxy nanocomposite covered with Kapton on both sides, placed in aluminum housings

The housings and lids were numbered and weighed right before and after the test to notice and difference in their masses. Figure 6.6 (a) and figure 6.6 (b) shows housing and specimen being weighed and figure 6.6 (c) shows housing after specimen being placed and covered with lid.

Each test specimen was weighed and kept in clean and pre-weighed aluminum boats. These were then covered with lids and kept in the vacuum chamber. Pressure was slowly reduced to approximately 5×10^{-3} torr and maintained for 24 hours at room temperature. After the test, the pressure was slowly brought down to atmospheric pressure and the test specimen, aluminum housings and lids were weighed separately to check for any differences. Weights of specimen before and after the test are taken separately. Four quantity of each type of sample were tested and their averaged TML values found are given in Table 6.2. The averaged TML values of these three types of nanocomposites are shown in Figure 6.7.

Figure 6.6 (a) Weighing of boat (b) weighing of test specimen (c) housing covered with lid.

Table 6.2 TML values of four samples of each type of specimen

Material	TML
CNT/2216 Trans epoxy	0.40
	0.11
	0.04
	0.45
CNT+GP/2216 Trans epoxy	0.60
	0.20
	0.00
	0.65
CNT+GP/2216 Trans epoxy/Kapton	0.30
	0.67
	0.18
	0.36
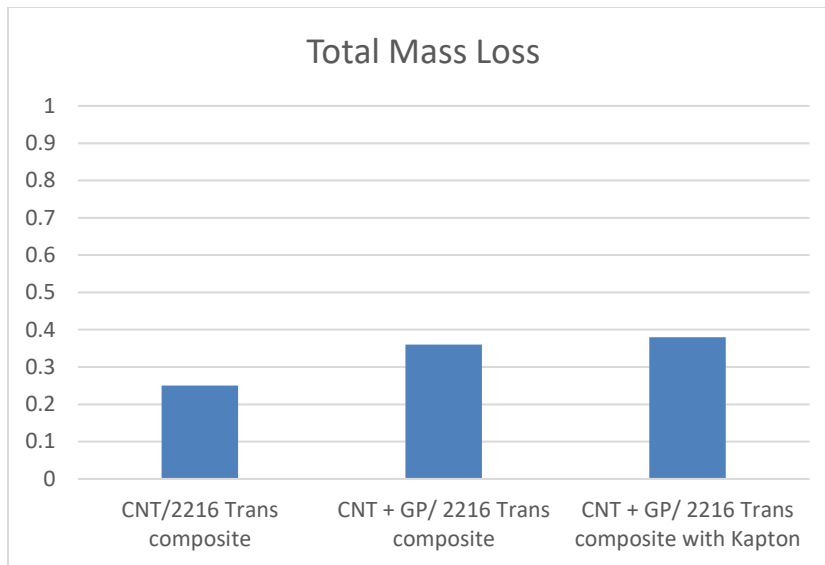
Figure 6.7 Averaged TML values of different nanocomposities

Mass loss has been observed in all types of test specimen after outgassing testing. TML values of all composite materials tested are found to be less than 1% in this test. It is observed that with increase in constituent materials in the nanocomposite, the TML values is increased. Limitations in the test setup such as isolation of specimen from each other during the test, accuracy and reliability of weighing scale etc. are the factors that can arise abnormality in the values and should be improved. Higher TML values are expected at tests conducted at lower vacuum levels and higher temperatures.

7. Conclusion

In this study CNT+GNP/epoxy based hybrid nanocomposites have been developed, characterized and used for sensing of strains, vibrations and damage. Different types of epoxy matrices have been tested and compared to improve the strain sensing range and the piezoresistive response of the nanocomposites. The results shows that CNT+GNP/2216 Translucent epoxy composites yeild much flexible sensors, which can undergo up to 11% strains, and show 5 times higher piezoresistive response than the previous CNT+GNP/WS epoxy based nanocomposites.

Vibration testing have been done in order to investigate the response for cyclic loading. It has been shown that the piezoresistive sensor is able to change in resistance as the applied strains vary during each vibration cycles. Effect of change in amplitude and frequency of the response have been investigated and positive results have been achieved for frequency range up to 50 Hz, showing their potential of as vibration sensors. Digital image correlation technique has been used to investigate the strain variation within the specimen both in static and dynamic loading.

Dynamic mechanical analysis has been performed to characterize the viscoelastic behavior of the nanocomposite due to epoxy matrix. Variation of elastic modulus and glass transition temperatures at different frequencies and temperatures have been obtained and both temperature and frequency dependence is observed. Glass transition temperature is found to be around $51^{o}C$ at 1 Hz and elastic behavior till $70^{o}C$ at room temperature.

The specimen have been tested for detection of damage caused by micrometeoroid and orbital debris by addition of holes. The sensors have a linear and stable response to the

damage and can be used as thin flexible film inside the layers of walls of inflatable structure, when coated with Kapton on both sides. A computer program has been developed to detect the occurrence of damage, size of damage, its location and depth of penetration for active structural health monitoring of the structure. Apparatus has been designed to conduct outgassing testing according to ASTM standard to validate the suitability of these nanocomposite sensors in vacuum environment. The total mass loss of the material is found to be less than 1% under given test conditions which is within the range of recommended space materials. Hence these developed nanocomposites have significant potential to be used as strain sensors, vibration sensors and damage detection sensors for MMOD impacts.

8. Recommendations

1. In development of nanocomposites, GNP are obtained by manually cutting of graphene sheet using knife blade. This process is time consuming and does not give uniform size platelets which greatly affects the piezoresistive response. An automated process for cutting e.g. laser cutting should be used to obtain uniform shape and size particles.

2. Application of GNP + epoxy mixture on the bucky paper is also manual and there is no control to measure the amount of mixture in each specimen. Difference in amount of GNP + epoxy mixture on buckypaper greatly affects the resistance and piezoresistive behavior. Some sort of device such as epoxy applicator, spray gun, etc. should be used to control the amount of mixture on the buckypaper.

3. Outgassing testing shall be performed using ASTM recommended procedure and apparatus to yield more reliable results.

REFERENCES

3M. 2009. "Scotch-Weld Epoxy Adhesive 2216 B/A." *Datasheet* Dec.

Abdel-Goad, Mahmoud, and Petra Pötschke. 2005. "Rheological Characterization of Melt Processed Polycarbonate-Multiwalled Carbon Nanotube Composites." *Journal of Non-Newtonian Fluid Mechanics* 128(1 SPEC. ISS.): 2–6.

Aldraihem, Osama J., Wael N. Akl, and Amr M. Baz. 2009. "Nanocomposite Functional Paint Sensor for Vibration and Noise Monitoring." *Sensors and Actuators, A: Physical* 149(2): 233–40.

Anees, Muhammad, Audrey Gbaguidi, Daewon Kim, and Sirish Namilae. 2017. "Structural Health Monitoring of Inflatable Structures for MMOD Impacts." *SPIE Smart Structures and Materials+ Nondestructive Evaluation and Health Monitoring*: 101690D–101690D.

"Application Note AN -708 Vibration Measurements with the Vibration Synchronization Module." http://www.correlatedsolutions.com/wp-content/uploads/2013/10/Fatigue-Vibration-Application_Note.pdf (October 30, 2017).

Aqel, Ahmad, Kholoud M.M. Abou El-Nour, Reda A.A. Ammar, and Abdulrahman Al-Warthan. 2012. "Carbon Nanotubes, Science and Technology Part (I) Structure, Synthesis and Characterisation." *Arabian Journal of Chemistry* 5(1): 1–23. http://linkinghub.elsevier.com/retrieve/pii/S1878535210001747 (October 31, 2017).

ASTM. 2011. "ASTM D4496.24781-Standard Test Method for D-C Resistance or Conductance of Moderately Conductive Materials." *Test* 87(Reapproved 1998): 2–6.

IEEE. 2012. "D257-14 Standard Test Methods for DC Resistance or Conductance of Insulating Materials 1." *Standard* i(C): 1–18.

ASTM. 2015. "E595 − 15 Standard Test Method for Total Mass Loss and Collected Volatile Condensable Materials from Outgassing in a Vacuum Environment (E595-07)." *Astm* i(July): 1–9.

Bokobza, Liliane. 2007. "Multiwall Carbon Nanotube Elastomeric Composites: A Review." *Polymer* 48(17): 4907–20. http://dx.doi.org/10.1016/j.polymer.2007.06.046.

Brandon, Erik J. et al. 2011. "Structural Health Management Technologies for

Inflatable/deployable Structures: Integrating Sensing and Self-Healing." *Acta Astronautica* 68(7–8): 883–903. http://dx.doi.org/10.1016/j.actaastro.2010.08.016.

C. Stampfer, *,† et al. 2006. "Nano-Electromechanical Displacement Sensing Based on Single-Walled Carbon Nanotubes." http://pubs.acs.org/doi/abs/10.1021/nl0606527 (October 26, 2017).

Cadogan, David et al. 2006. "Intelligent Flexible Materials for Deployable Space Structures (InFlex)." *Components* (May): 1–17. http://papers.sae.org/2006-01-2065/.

Chang, Chi-Yung et al. "Alignment and Properties of Carbon Nanotube Buckypaper/liquid Crystalline Polymer Composites." *Journal of Applied Polymer Science* 128(3): n/a-n/a. http://doi.wiley.com/10.1002/app.38209 (October 26, 2017).

Chapartegui, M et al. 2013. "Manufacturing, Characterization and Thermal Conductivity of Epoxy and Benzoxazine Multi-Walled Carbon Nanotube Buckypaper Composites." *Journal of Composite Materials* 47(14): 1705–15. http://journals.sagepub.com/doi/10.1177/0021998312450929 (October 26, 2017).

Christiansen, Eric L. 2009. "Handbook for Designing MMOD Protection." *NASA/TM–2009–214785* (June).

Christiansen, Eric L, and Mike Rollins. 2012. "MMOD Risk/External Inspection Needs for Re-Entry TPS." *NASA 20090010053*.

Coleman, Jonathan N. et al. 2003. "Improving the Mechanical Properties of Single-Walled Carbon Nanotube Sheets by Intercalation of Polymeric Adhesives." *Applied Physics Letters* 82(11): 1682–84. http://aip.scitation.org/doi/10.1063/1.1559421 (October 26, 2017).

David Gendron, Albert o Ansaldo, Grzegorz Bubak, Luca Ceseracciu, George Vamvounis, Davide Ricc. 2015. "Poly(ionic Liquid)-Carbon Nanotubes Self-Supported, Highly Electroconductive Composites and Their Application in Electroactive Devices." *Composites Science and Technology* 117: 364–70. https://www.sciencedirect.com/science/article/pii/S0266353815300476 (October 26, 2017).

Es, J S C, and Gerard D Valle. 2012. "Inflatable Module Inspection Needs Workshop Session 5-4." (281).

Fuente, H. de la, J. Raboin, G.R. Spexarth, and G.D. Valle. 2000. "TransHab: NASA's Large-Scale Inflatable Spacecraft." *2000 AIAA Space Inflatables Forum; Structures, Structural Dynamics, and Materials Conference* (April): 1–9. http://ntrs.nasa.gov/search.jsp?R=20100042636.

Gbaguidi, Audrey, Muhammad Anees, Sirish Namilae, and Daewon Kim. 2017. "Dynamic Piezoresistive Response of Hybrid Nanocomposites." In ed. Jerome P. Lynch. International Society for Optics and Photonics, 1016817. http://proceedings.spiedigitallibrary.org/proceeding.aspx?doi=10.1117/12.2260208 (October 7, 2017).

Gojny, Florian H., and Karl Schulte. 2004. "Functionalisation Effect on the Thermo-Mechanical Behaviour of Multi-Wall Carbon Nanotube/epoxy-Composites." *Composites Science and Technology* 64(15 SPEC. ISS.): 2303–8.

Gullapalli, Hemtej et al. 2010. "Flexible Piezoelectric ZnO – Paper Nanocomposite Strain Sensor." : 1641–46.

Hu, Ning et al. 2010. "Investigation on Sensitivity of a Polymer/carbon Nanotube Composite Strain Sensor." *Carbon* 48(3): 680–87. http://linkinghub.elsevier.com/retrieve/pii/S0008622309006824 (October 26, 2017).

Huang, Ya-Ting et al. 2012. "Design and Fabrication of Single-Walled Carbon Nanonet Flexible Strain Sensors." *Sensors* 12(12): 3269–80. http://www.ncbi.nlm.nih.gov/pubmed/22737007 (October 26, 2017).

IEEE. 2009. *62624-2009 Test Methods for Measurement of Electrical Properties of Carbon Nanotubes.* http://ieeexplore.ieee.org/document/5782922/ (October 27, 2017).

Inpil Kang a, Yun Yeo Heung a, Jay H. Kim b, Jong Won Lee d, Ramanand Gollapudi a, Srinivas Subramaniam c, Suhasini Narasimhadevara a, Douglas Hurd a, and Marina Ruggles-Wren Goutham R. Kirikera a, Vesselin Shanov c, Mark J. Schulz a,*, Donglu Shi c, Jim Boerio c, Shankar Mall e. 2006. "Introduction to Carbon Nanotube and Nanofiber Smart Materials." *Composites: Part B* 149(1): 233–40. http://www.mdpi.com/1424-8220/14/6/10042/ (February 6, 2017).

Jeffrey L. Bahr et al. 2001. "Functionalization of Carbon Nanotubes by Electrochemical Reduction of Aryl Diazonium Salts: A Bucky Paper Electrode." http://pubs.acs.org/doi/abs/10.1021/ja010462s (October 27, 2017).

Jihun Hwang, Jaeyoung Jang. Kipyo Hong, Kun Nyun Kim, Jong HunHan, Kwonwoo Shin, Chan Eon. 2011. "Poly(3-Hexylthiophene) Wrapped Carbon Nanotube/poly(dimethylsiloxane) Composites for Use in Finger-Sensing Piezoresistive Pressure Sensors." *Carbon* 49(1): 106–10. http://www.sciencedirect.com/science/article/pii/S000862231000624X (October 26, 2017).

Joung-Man Park, Ga-Young Gu, Zuo-Jia Wang, Dong-Jun Kwon, K. LawrenceDeVries. 2013. "Interfacial Durability and Electrical Properties of CNT or ITO/PVDF Nanocomposites for Self-Sensor and Micro Actuator Applications." *Applied Surface Science* 287: 75–83. http://www.sciencedirect.com/science/article/pii/S0169433213017108 (October 26, 2017).

Kang, InpilKim, Schulz, Mark J, Kim, Jay H, Vesselin Shanov, and Donglu Shi. 2006. "A Carbon Nanotube Strain Sensor for Structural Health Monitoring." *SMARTMATERIALS AND STRUCTURES* 15.

Kang, Inpil et al. 2006. "Introduction to Carbon Nanotube and Nanofiber Smart Materials." *Composites Part B: Engineering* 37(6): 382–94.

Kon, Stanley, Kenn Richard Oldham, and Roberto Horowitz. 2007. "Piezoresistive and Piezoelectric MEMS Strain Sensors for Vibration Detection." *SPIE_International Society for Optical Engineering (SPIE)* 6529: 65292V–65292V–11. http://link.aip.org/link/PSISDG/v6529/i1/p65292V/s1&Agg=doi%5Cnhttp://spiedigitallibrary.org/proceeding.aspx?doi=10.1117/12.715814%5Cnhttp://proceedings.spiedigitallibrary.org/proceeding.aspx?articleid=1301155.

Koshti, Ajay M. 2015. "Considerations for Ultrasonic Testing Application for on-Orbit NDE." *SPIE Smart Structures and Materials + Nondestructive Evaluation and Health Monitoring*: 94372H. http://proceedings.spiedigitallibrary.org/proceeding.aspx?articleid=2239084.

Lewis, Mark E, and Merritt Island. 2016. "Multi-Dimensional Damage Detection." (12).

Li, Jing, Pui Shan Wong, and Jang Kyo Kim. 2008. "Hybrid Nanocomposites Containing Carbon Nanotubes and Graphite Nanoplatelets." *Materials Science and Engineering A* 483–484(1–2 C): 660–63.

Li, Jiukun, and Sirish Namilae. 2016. "Nanotube Sheet — Graphite Hybrid

Nanocomposite for Damage Detection." In *TMS 2016 145th Annual Meeting & Exhibition*, Cham: Springer International Publishing, 69–76. http://link.springer.com/10.1007/978-3-319-48254-5_9 (February 24, 2017).

Li, Xiaodong et al. 2004. "Nanomechanical Characterization of Single-Walled Carbon Nanotube Reinforced Epoxy Composites." *Nanotechnology* 15(11): 1416–23. http://stacks.iop.org/0957-4484/15/i=11/a=005?key=crossref.202080bb095df75f11c3316ad951aaa9 (September 22, 2017).

Li, Zhongrui, Rebekah Downes, and Zhiyong Liang. 2015. "In Situ Polymerized pCBT Composites with Aligned Carbon Nanotube Buckypaper: Structure and Properties." *Macromolecular Chemistry and Physics* 216(3): 292–300. http://doi.wiley.com/10.1002/macp.201400443 (October 26, 2017).

Loh, Kenneth J et al. 2007. "Multifunctional Layer-by-Layer Carbon Nanotube–polyelectrolyte Thin Films for Strain and Corrosion Sensing." *Smart Materials and Structures* 16(2): 429–38. http://stacks.iop.org/0964-1726/16/i=2/a=022?key=crossref.68459f15e81c4209e66926f3b4c82bb6 (October 26, 2017).

M.Chapartegui, J.Barcena, X.Irastorza, C.Elizetxea, M.Fernandez, A.Santamaria. 2012. "Analysis of the Conditions to Manufacture a MWCNT Buckypaper/benzoxazine Nanocomposite." *Composites Science and Technology* 72(4): 489–97. http://www.sciencedirect.com/science/article/pii/S0266353811004271 (October 26, 2017).

Madaras, Eric I et al. 2008. "The Potential for Imaging in Situ Damage in Inflatable Space Structures." *AIP Conference Proceedings*.

Manchado, M. A López, L. Valentini, J. Biagiotti, and J. M. Kenny. 2005. "Thermal and Mechanical Properties of Single-Walled Carbon Nanotubes-Polypropylene Composites Prepared by Melt Processing." *Carbon* 43(7): 1499–1505.

McCook, N. L., M. A. Hamilton, D. L. Burris, and W. G. Sawyer. 2007. "Tribological Results of PEEK Nanocomposites in Dry Sliding against 440C in Various Gas Environments." *Wear* 262(11–12): 1511–15.

Meyers, Marc André, and Krishan Kumar Chawla. 2009. *Mechanical Behavior of Materials*. http://www.smesfair.com/pdf/mechanical eng/smesfair09.pdf.

Micheli, Davide et al. 2012. "Temperature, Atomic Oxygen and Outgassing Effects on Dielectric Parameters and Electrical Properties of Nanostructured Composite Carbon-Based Materials." *Acta Astronautica* 76: 127–35. http://dx.doi.org/10.1016/j.actaastro.2012.02.019.

Mittal, Vikas. 2011. *Nanocomposites with Biodegradable Polymers : Synthesis, Properties, and Future Perspectives*. Oxford University Press.

Ogasawara, Toshio, Yuichi Ishida, Takashi Ishikawa, and Rikio Yokota. 2004. "Characterization of Multi-Walled Carbon Nanotube/phenylethynyl Terminated Polyimide Composites." *Composites Part A: Applied Science and Manufacturing* 35(1): 67–74.

Pham, Giang T et al. 2008. "Mechanical and Electrical Properties of Polycarbonate Nanotube Buckypaper Composite Sheets." *Nanotechnology* 19(32): 325705. http://www.ncbi.nlm.nih.gov/pubmed/21828827 (October 26, 2017).

Powers, Charles E. "Outgassing Data for Selecting Spacecraft Materials System." https://outgassing.nasa.gov/ (October 16, 2017).

Rajoria, Himanshu, and Nader Jalili. 2005. "Passive Vibration Damping Enhancement Using Carbon Nanotube-Epoxy Reinforced Composites." *Composites Science and Technology* 65(14): 2079–93.

Shaffer, Milo S P, and Alan H. Windle. 1999. "Fabrication and Characterization of Carbon Nanotube/poly(vinyl Alcohol) Composites." *Advanced Materials* 11(11): 937–41.

Sham, Man Lung, and Jang Kyo Kim. 2006. "Surface Functionalities of Multi-Wall Carbon Nanotubes after UV/Ozone and TETA Treatments." *Carbon* 44(4): 768–77.

Sreekumar, T. V. et al. 2003. "Single-Wall Carbon Nanotube Films." *Chemistry of Materials* 15(1): 175–78. http://pubs.acs.org/doi/abs/10.1021/cm020367y (October 26, 2017).

Studor, and George. 2007. "Lessons Learned JSC Micro-Wireless Instrumentation Systems on Space Shuttle and International Space Station CANEUS 2006."

Sung, Y.T. et al. 2005. "Dynamic Mechanical and Morphological Properties of Polycarbonate/multi-Walled Carbon Nanotube Composites." *Polymer* 46(15): 5656–

61. http://linkinghub.elsevier.com/retrieve/pii/S0032386105005616.

Thostenson, E. T., and T.-W. Chou. 2006. "Carbon Nanotube Networks: Sensing of Distributed Strain and Damage for Life Prediction and Self Healing." *Advanced Materials* 18(21): 2837–41. http://doi.wiley.com/10.1002/adma.200600977 (October 26, 2017).

Vail, J. R., D. L. Burris, and W. G. Sawyer. 2009. "Multifunctionality of Single-Walled Carbon Nanotube-Polytetrafluoroethylene Nanocomposites." *Wear* 267(1–4): 619–24.

Velasco-Santos, C et al. 2003. "Dynamical – Mechanical and Thermal Analysis of Carbon Nanotube – Methyl-Ethyl Methacrylate Nanocomposites." *Journal of Physics D: Applied Physics* 36: 1423–28.

"Vic-3D 2010." http://www.correlatedsolutions.com/installs/Vic-3D-2010-manual.pdf (October 30, 2017).

Wang, Sheng. 2005. "Characterization and Analysis of Electrical Conductivity Properties of Nanotube   Composites." http://diginole.lib.fsu.edu/islandora/object/fsu%3A175807 (October 26, 2017).

Woodard, Stanley E. et al. 2011. "Method to Have Multilayer Thermal Insulation Provide Damage Detection." *Journal of Spacecraft and Rockets* 48(6): 920–30. http://arc.aiaa.org/doi/abs/10.2514/1.44400.

Xia, Hesheng, and Mo Song. 2005. "Preparation and Characterization of Polyurethane–carbon Nanotube Composites." *Soft Matter* 1(5): 386.

Xiong, Jiawen et al. 2006. "The Thermal and Mechanical Properties of a Polyurethane/multi-Walled Carbon Nanotube Composite." *Carbon* 44(13): 2701–7.

Xu, Lihua, Zhengping Fang, Ping'an Song, and Mao Peng. 2010. "Functionalization of Carbon Nanotubes by Corona-Discharge Induced Graft Polymerization for the Reinforcement of Epoxy Nanocomposites." *Plasma Processes and Polymers* 7(9–10): 785–93. http://dx.doi.org/10.1002/ppap.201000019.

Yin, Gang et al. 2011. "A Carbon Nanotube/polymer Strain Sensor with Linear and Anti-Symmetric Piezoresistivity."

Yuezhen Bin, Mayuna Kitanaka, and Dan Zhu, and Masaru Matsuo*. 2003. "Development of Highly Oriented Polyethylene Filled with Aligned Carbon Nanotubes by Gelation/Crystallization from Solutions." http://pubs.acs.org/doi/abs/10.1021/ma0301956 (October 26, 2017).

Zhao, Haibo et al. 2010. "Carbon Nanotube Yarn Strain Sensors." *Nanotechnology* 21(30): 305502. http://stacks.iop.org/0957-4484/21/i=30/a=305502?key=crossref.28dfad3d57d1e6c19995c1f36aa89f6a (October 26, 2017).